Inorganic Chemistry

Article

pubs.acs.org/IC

Synthesis, Characterization, and Some Properties of Cp*W(NO)(H)(η^3-allyl) Complexes

Rhett A. Baillie,[†] Aaron S. Holmes,[†] Guillaume P. Lefèvre,[†] Brian O. Patrick,[†] Monica V. Shree,[†] Russell J. Wakeham,[†] Peter Legzdins,*[,†] and Devon C. Rosenfeld[‡]

[†]Department of Chemistry, The University of British Columbia, Vancouver, British Columbia, Canada V6T 1Z1

[‡]The Dow Chemical Company, 2301 North Brazosport Boulevard, Freeport, Texas 77541, United States

Supporting Information

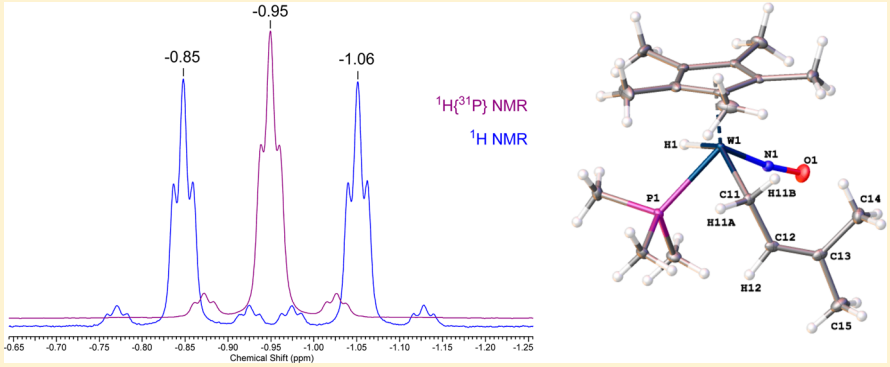

ABSTRACT: Sequential treatment at low temperatures of Cp*W(NO)Cl_2 in THF with 1 equiv of a binary magnesium allyl reagent, followed by an excess of $LiBH_4$, affords three new Cp*W(NO)(H)(η^3-allyl) complexes, namely, Cp*W(NO)(H)(η^3-CH_2CHCMe_2) (**1**), Cp*W(NO)(H)(η^3-$CH_2CHCHPh$) (**2**), and Cp*W(NO)(H)(η^3-$CH_2CHCHMe$) (**3**). Complexes **1**−**3** are isolable as air-stable, analytically pure yellow solids in good to moderate yields by chromatography or fractional crystallization. In solutions, complex **1** exists as two coordination isomers in an 83:17 ratio differing with respect to the *endo*/*exo* orientation of the allyl ligand. In contrast, complexes **2** and **3** each exist as four coordination isomers, all differing by the orientation of their allyl ligands which can have either an *endo* or an *exo* orientation with the phenyl or methyl groups being either proximal or distal to the nitrosyl ligand. A DFT computational analysis using the major isomer of Cp*W(NO)(H)(η^3-$CH_2CHCHMe$) (**3a**) as the model complex has revealed that its lowest-energy thermal-decomposition pathway involves the intramolecular isomerization of **3a** to the 16e η^2-alkene complex, Cp*W(NO)(η^2-CH_2═$CHCH_2Me$). Such η^2-alkene complexes are isolable as their 18e PMe_3 adducts when compounds **1**−**3** are thermolyzed in neat PMe_3, the other organometallic products formed during these thermolyses being Cp*W(NO)$(PMe_3)_2$ (**5**) and, occasionally, Cp*W(NO)(H)(η^1-allyl)(PMe_3). All new complexes have been characterized by conventional spectroscopic and analytical methods, and the solid-state molecular structures of most of them have been established by single-crystal X-ray crystallographic analyses.

INTRODUCTION

We have recently been investigating the family of Cp*W(NO)(alkyl)(η^3-allyl) [Cp* = η^5-C_5Me_5] complexes, which initiate various types of hydrocarbon C−H activations.[1] Specifically, gentle thermolyses of Cp*W(NO)(CH_2CMe_3)(η^3-allyl) complexes in neat hydrocarbon solutions result in the loss of neopentane from the metal's coordination spheres and the transient formation of the 16-electron (16e) intermediate species Cp*W(NO)(η^2-allene) and/or Cp*W(NO)(η^2-diene). These transient intermediates can react with hydrocarbon substrates, RH (R = alkyl, aryl), to form three different types of organometallic products, as summarized in Scheme 1.[2]

It is notable that two of the three types of complexes resulting from the C−H activation of various hydrocarbons by Cp*W(NO)(CH_2CMe_3)(η^3-allyl) complexes are Cp*W(NO)(H)(η^3-allyl) compounds, which constitute a new family of hydrido nitrosyl complexes, a class of compounds whose chemistry has not been extensively investigated. Consequently, we decided to synthesize some of these Cp*W(NO)(H)(η^3-allyl) complexes independently, to characterize them fully by conventional spectroscopic methods, and to establish the solid-state molecular structures of several of them. Finally, we set out to establish some of their characteristic physical and chemical properties to see how they compared to those exhibited by their Cp*W(NO)(CH_2CMe_3)(η^3-allyl) precursors. In this Article, we present the initial results of our investigations.

Received: April 2, 2015
Published: May 22, 2015

ACS Publications © 2015 American Chemical Society

DOI: 10.1021/acs.inorgchem.5b00747
Inorg. Chem. 2015, 54, 5915−5929

Scheme 1. C−H Activations Effected by Cp*W(NO)(CH_2CMe_3)(η^3-allyl) Complexes

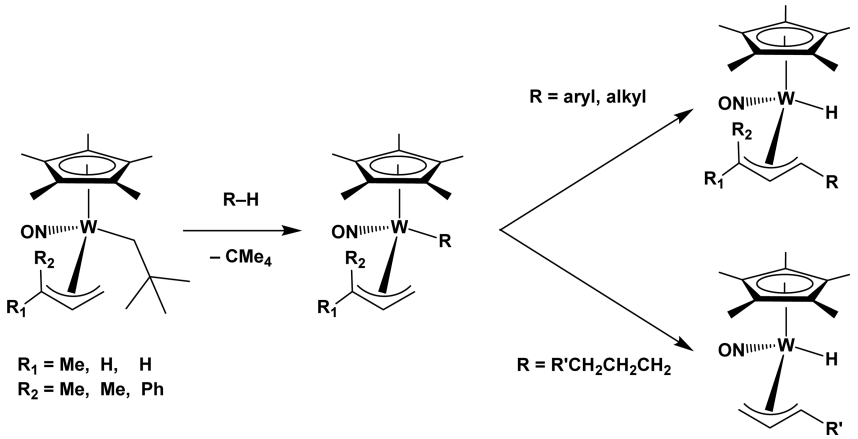

Scheme 2. Synthesis of Cp*W(NO)(H)(η^3-CH_2CHCMe_2) (1)

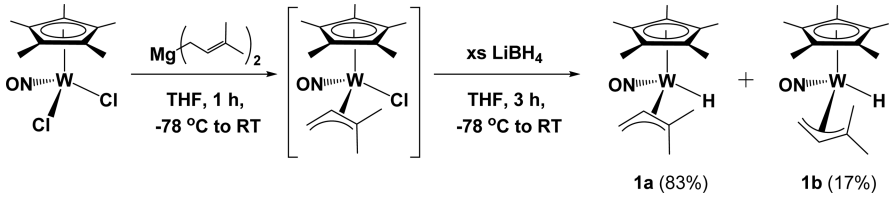

RESULTS AND DISCUSSION

Synthesis and Characterization of the Hydride Complexes. Syntheses of the family of Cp*W(NO)(H)(η^3-allyl) complexes all proceed in a similar fashion from Cp*W(NO)Cl_2, the allyl and hydride ligands being installed sequentially via salt metatheses. The specific conditions employed for the preparation of the two isomers of Cp*W(NO)(H)(η^3-CH_2CHCMe_2) (**1**) are summarized in Scheme 2.

In general, the addition of the appropriate binary magnesium(II) allyl reagent to Cp*W(NO)Cl_2 is carried out at −78 °C and under a N_2 atmosphere. The choice of solvent is critical since, under the experimental conditions employed, Cp*W(NO)Cl_2 is only sparingly soluble in THF and not at all in Et_2O. After the addition of the allylating reagent is complete, the reaction mixture is allowed to warm to room temperature while being stirred for at least 1 h to produce the intermediate complex, Cp*W(NO)(η^3-allyl)Cl. These 18e intermediate complexes can be isolated, but such isolation is not necessary for the synthesis (and can even diminish the overall yield) of the Cp*W(NO)(H)(η^3-allyl) compounds. The reaction mixture containing Cp*W(NO)(η^3-allyl)Cl is next cooled in a dry ice/acetone bath, an excess of $LiBH_4$ is added slowly, and the mixture is allowed to stir for at least 3 h. A variety of different hydride reagents have been investigated (e.g., $LiAlH_4$, $NaBH_4$, etc.), and while others produced the desired Cp*W(NO)(H)(η^3-allyl) complexes, $LiBH_4$ gave more consistent results and higher yields of the hydrides.

The purification of the Cp*W(NO)(H)(η^3-allyl) complexes can be effected on the bench since they have a surprising degree of air and moisture stability. The excess $LiBH_4$ is first neutralized with water in Et_2O, and then the salts are removed by filtration. The mixture is then subjected to column chromatography on a neutral alumina support to obtain analytically pure Cp*W(NO)(H)(η^3-allyl) complexes. Complexes **1** and Cp*W(NO)(H)(η^3-$CH_2CHCHPh$) (**2**) are isolable as yellow solids in yields of 45% and 20%, respectively, by removing solvent from the eluate in vacuo. The third complex, Cp*W(NO)(H)(η^3-$CH_2CHCHMe$) (**3**), must be recrystallized from cold hexanes in order to obtain a pure, yellow solid in 19% yield. The melting points of **1**−**3** are reversible; this has been established by dissolving the melt residue in C_6D_6 and analyzing each sample by ^1H NMR spectroscopy. In each case, the ^1H NMR spectrum matches the spectrum for the respective starting hydride complex. Interestingly, there is a 50 °C difference between the highest and lowest melting points of these three compounds. The lowest melting point belongs to **3** (75−78 °C), the highest to **1** (123−125 °C), and **2** has an exactly intermediate melting point (99−100 °C). All three complexes **1**−**3** are air- and moisture-stable in the solid state for several weeks. In solution, however, they are slightly less stable, and a small degree of decomposition occurs after several days both in air and under N_2.

Complex **1** exists as two coordination isomers in an 83:17 ratio in C_6D_6 solution (Scheme 2) that differ with respect to the *endo*/*exo* orientation of their allyl ligands. The solution molecular structures have been determined using Sel NOE and NOESY NMR spectroscopy. The selective irradiation of the signals due to the hydride ligands results in NOE enhancement of both allyl *Me* signals for each isomer [i.e., δ irrad. −0.90 ppm, NOE at 1.90 ppm, 2.29 ppm; δ irrad. −0.59 ppm, NOE at 0.87 ppm, 2.45 ppm]. The *exo* conformation of the allyl ligand of the major isomer is established by the NOESY NMR spectrum, which displays cross-peaks between the signals due to the C_5Me_5 ligand and the allyl *meso H* (1.72, 2.68 ppm) and the C_5Me_5 ligand and the allyl *H* that is *cis* to the *meso H* (1.72, 2.06 ppm).

Complexes **2** and **3** each exist as four coordination isomers in solution, all differing by the orientation of the allyl ligand, which can have either an *endo* or an *exo* orientation with the phenyl/methyl groups, as shown in Figure 1. The solution

DOI: 10.1021/acs.inorgchem.5b00747
Inorg. Chem. 2015, 54, 5915−5929

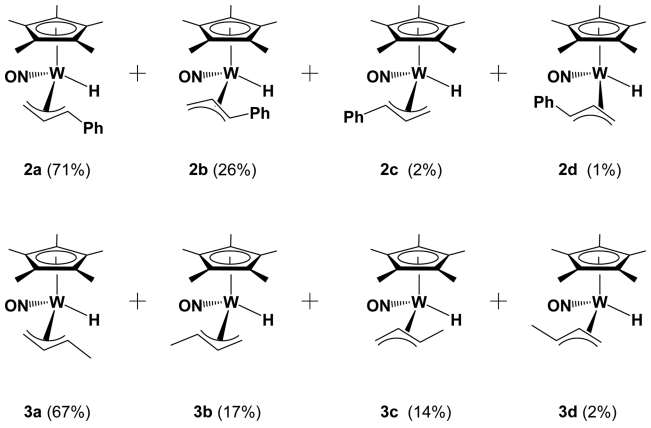

Figure 1. Solution molecular structures of the isomers of **2** and **3** as determined by ^{1}H Sel NOE NMR spectroscopy.

molecular structures of the isomers have also been determined using NOE NMR spectroscopy. Interestingly, there is a correlation between the *endo*/*exo* orientation of the allyl ligand and the chemical shift of the allyl *meso H* in the ^{1}H NMR spectra for each complex. For a given complex, the *meso H* signals of the *endo* isomers have a more downfield chemical shift in the ^{1}H NMR spectra than do the *meso H* signals of the *exo* isomers (Table 1), presumably because of their differing interactions with the tungsten centers.

Table 1. ^{1}H NMR Chemical Shifts (δ) in ppm of the Allyl *meso H* Signals for 1−3 in C_6D_6 Highlighting the Relative Differences between the *endo* and *exo* Orientations of the Allyl Ligands in the Isomers

	complex **1**	complex **2**	complex **3**
endo	**1b**; 4.71	**2a**; 5.36	**3a**; 4.61
		2c; 5.03	**3b**; 4.35
exo	**1a**; 2.68	**2b**; 3.76	**3c**; 2.82
		2d; 4.33	**3d**; 2.48

The solid-state molecular structures of **1**−**3** have been established by X-ray crystallographic analyses. Only a single isomer of **1** has been observed in the solid state (Figure 2), and it is **1a**, the major isomer in solution. The allyl ligand is in an *exo* conformation, and its CMe_2 substituent is *cis* to the smaller hydride ligand instead of the larger nitrosyl ligand, consistent with the NOE and NOESY NMR data. As expected, the allyl ligand also exhibits a slight σ−π distortion, a manifestation of the electronic asymmetry extant at the metal center.[3,4] The ^{1}H and ^{13}C NMR spectra of **1a** in C_6D_6 indicate that its solid-state molecular structure persists in solution. The minor isomer **1b** evidently does not cocrystallize with the major isomer during the growth of X-ray-quality crystals of **1a** from Et_2O at −33 °C. In any event, dissolution of a crystalline sample of **1a** in C_6D_6 produces a solution containing both isomers in the same 83:17 equilibrium ratio. All solution reactions of **1** have been performed with similar mixtures of these isomers. Similarly, the solution isomers of **2** and **3** shown in Figure 1 are unchanging equilibrium mixtures that have also been used in all further chemical investigations.

The crystal structure of **2** consists of the packing of two isomers, each displaying a three-legged piano-stool molecular geometry. In the molecular structure of the major isomer **2a** (Figure 3), the phenylallyl ligand is in an *endo* conformation

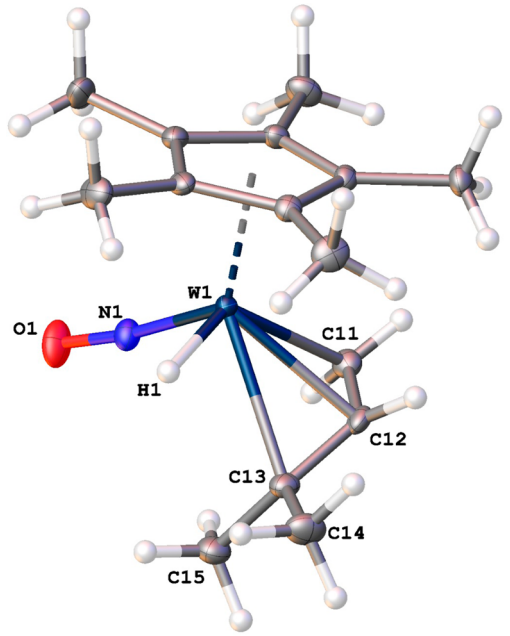

Figure 2. Solid-state molecular structure of **1a** with 50% probability thermal ellipsoids shown. Selected bond lengths (Å) and angles (deg): W(1)−H(1) = 1.62(3), W(1)−C(11) = 2.271(2), W(1)−C(12) = 2.287(2), W(1)−C(13) = 2.465(2), C(11)−C(12) = 1.419(3), C(12)−C(13) = 1.405(3), W(1)−N(1) = 1.7787(19), N(1)−O(1) = 1.228(2), C(11)−C(12)−C(13) = 124.7(2), C(12)−C(13)−C(14) = 117.5(2), C(12)−C(13)−C(15) = 123.1(2), W(1)−N(1)−O(1) = 173.62(18).

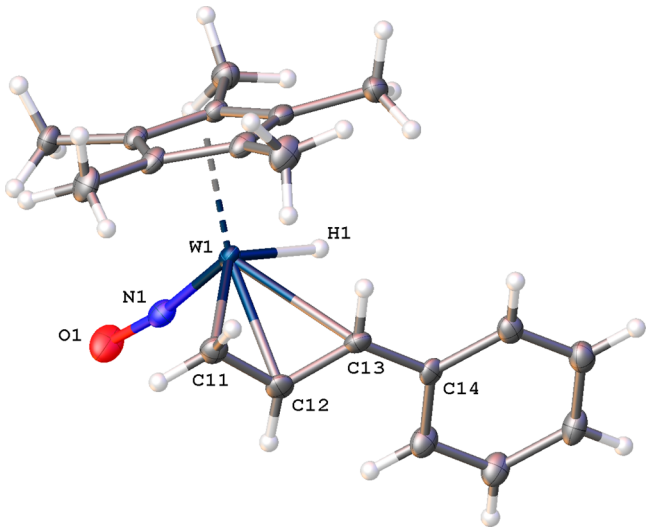

Figure 3. Solid-state molecular structure of **2a** having the phenylallyl ligand in the *endo* conformation with 50% probability thermal ellipsoids. Selected bond lengths (Å) and angles (deg): W(1)−H(1) = 1.76(4), W(1)−N(1) = 1.769(3), N(1)−O(1) = 1.235(4), W(1)−C(11) = 2.215(19), W(1)−C(12) = 2.313(6), W(1)−C(13) = 2.472(5), C(11)−C(12) = 1.412(18), C(12)−C(13) = 1.396(8), C(13)−C(14) = 1.483(6), W(1)−N(1)−O(1) = 171.1(3), C(11)−C(12)−C(13) = 120.2(9), C(12)−C(13)−C(14) = 126.0(5).

while the minor isomer **2b** (Figure 4) has the ligand in an *exo* conformation. Both isomers have the phenyl ring of the allyl ligand distal with respect to the nitrosyl ligand. This feature contrasts to that existing in $Cp^*W(NO)(CH_2CMe_3)(\eta^3$-$CH_2CHCHPh)$, which has the phenyl substituent in a proximal

DOI: 10.1021/acs.inorgchem.5b00747
Inorg. Chem. 2015, 54, 5915−5929

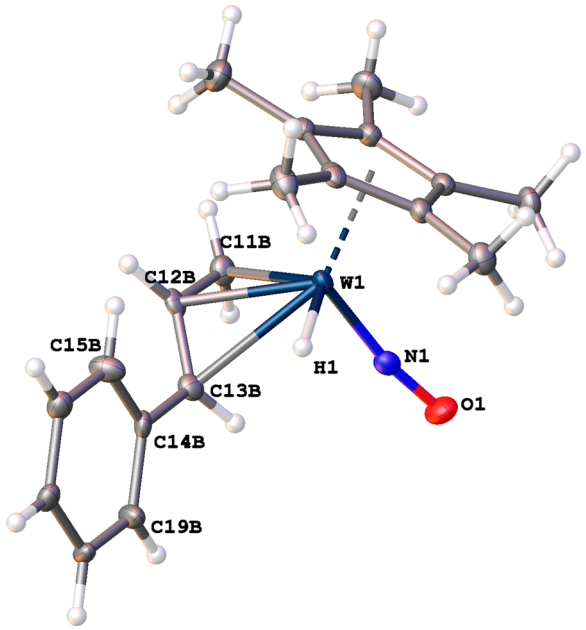

Figure 4. Solid-state molecular structure of **2b** with the phenylallyl ligand in the *exo* conformation with 50% probability thermal ellipsoids. Selected bond lengths (Å) and angles (deg): W(1)−H(1) = 1.76(4), W(1)−N(1) = 1.769(3), N(1)−O(1) = 1.235(4), W(1)−C(11b) = 2.31(6), W(1)−C(12b) = 2.302(16), W(1)−C(13b) = 2.526(13), C(11b)−C(12b) = 1.45(5), C(12b)−C(13b) = 1.39(2), C(13b)−C(14b) = 1.461(16), W(1)−N(1)−O(1) = 171.1(3), C(11b)−C(12b)−C(13b) = 121(3), C(12b)−C(13b)−C(14b) = 123.9(14).

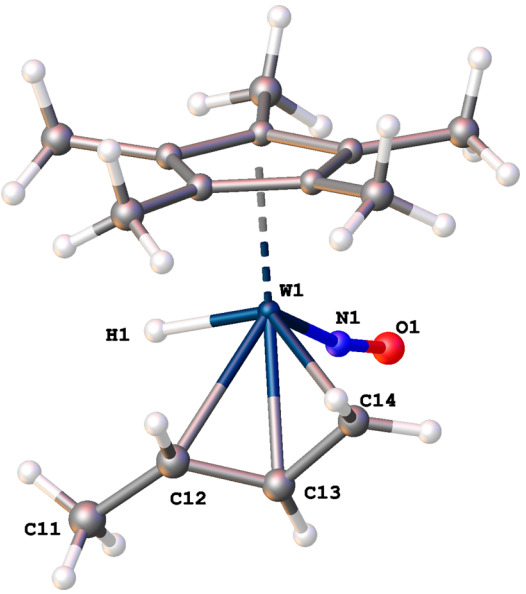

Figure 5. Solid-state molecular structure of **3a** with 50% probability thermal ellipsoids shown. Selected bond lengths (Å) and angles (deg.): W(1)−H(1) = 1.61(5), W(1)−C(12) = 2.400(4), W(1)−C(13) = 2.324(3), W(1)−C(14) = 2.250(3), C(11)−C(12) = 1.505(5), C(12)−C(13) = 1.376(5), C(13)−C(14) = 1.423(5), W(1)−N(1) = 1.781(3), N(1)−O(1) = 1.224(3), C(11)−C(12)−C(13) = 124.6(3), C(12)−C(13)−C(14) = 119.8(3), W(1)−N(1)−O(1) = 169.3(2).

configuration with respect to the NO group.[5] Presumably, the lack of steric interference of the hydride ligand in **2** allows the distal isomer to be more favorable in the hydride than in the alkyl allyl complex. Both isomers of **2** again show $\sigma-\pi$ distortion of the allyl ligand, although this effect is more pronounced in the *exo* isomer **2b**.

X-ray-quality crystals of **3** have been obtained via slow evaporation of an Et_2O solution of the compound at room temperature. The crystals contain only a single coordination isomer, namely, **3a**, which is also the major isomer in solution. The solid-state molecular structure of **3a** is shown in Figure 5. The allyl ligand is oriented in an *endo* conformation with the methyl substituent proximal to the hydride ligand. This feature is consistent with the ^{1}H NMR and Sel NOE NMR data for the isomer. The allyl ligand also exhibits a $\sigma-\pi$ distortion with the shorter C(12)−C(13) bond being *trans* to the nitrosyl ligand. This arrangement is likely a manifestation of the strong backbonding character of the nitrosyl ligand leaving less electron density at the W center to back-donate to the allyl C(12)−C(13) bond.

Theoretical Considerations. We have previously established that thermolyses of 18e Cp*W(NO)(CH_2CMe_3)(η^3-allyl) compounds result in the intramolecular elimination of CMe_4 and the formation of 16e η^2-diene and/or η^2-allene intermediate complexes that effect a variety of intermolecular C−H activations of hydrocarbons.[2] We, therefore, anticipated that the thermal decomposition of the related Cp*W(NO)(H)(η^3-allyl) complexes might involve the analogous intramolecular elimination of H_2 and the formation of the same 16e C−H activating intermediate species. However, a computational analysis using the major isomer of Cp*W(NO)(H)(η^3-$CH_2CHCHMe$) (**3a**) as the model complex has revealed that such is not the case (Scheme 3).

The lowest-energy thermal-decomposition pathway involves the intramolecular isomerization of **3a** to the 16e η^2-alkene complex, Cp*W(NO)(η^2-CH_2=$CHCH_2Me$). The corresponding η^2-diene and η^2-allene molecular hydrogen intermediate complexes are formed via significantly higher-energy pathways and hence are unlikely to be involved in the thermal chemistry exhibited by **3**.

In addition to employing DFT methods for delineating the probable thermal reaction mechanism employed by **3a**, we have also used an accurate method to compute the electronic structure of the complex.[6] The results of these calculations are summarized in terms of the electronic surface potential of **3a** shown in Figure 6. Not surprisingly, the negative charge is mainly located on the nitrosyl ligand (q(NO) = −0.196 |e|), whereas the charge borne by the hydrogen atom bound to the metal is close to zero (q(H) = 0.084 |e|). In other words, the slightly yellow-green color located around the W−H bond in Figure 6 attests that there is no excess charge (either positive or negative) located on this part of the molecule. A consequence of the absence of a strong negative charge on the hydrido ligand in **3a** is the stability of the complex in weakly acidic media such as water.

Reactions of the Hydride Complexes with PMe_3. As a first step in ascertaining the thermal behavior of the three hydride complexes **1**−**3**, they have been thermolyzed in the presence of PMe_3 to trap any coordinatively unsaturated organometallic species (such as the η^2-alkene complex shown in Scheme 3) that might be formed. Maintenance of a solution of **1** in neat trimethylphosphine at 60 °C for 18 h affords a mixture of two new organometallic complexes, namely, Cp*W(NO)(H)(η^1-CH_2CH=CMe_2)(PMe_3) (**4**) and Cp*W(NO)(PMe_3)$_2$ (**5**) in a ratio of 85:15 (Scheme 4). The two

DOI: 10.1021/acs.inorgchem.5b00747
Inorg. Chem. 2015, 54, 5915−5929

Scheme 3. Possible Thermal-Decomposition Pathways of 1

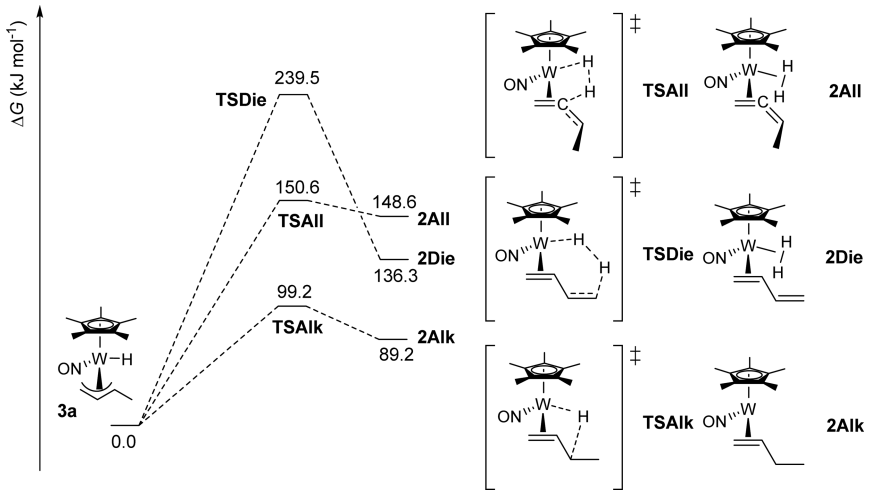

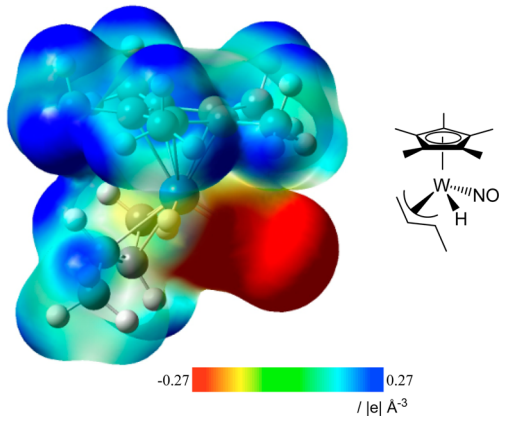

Figure 6. Computed electronic surface potential of the major isomer of Cp*W(NO)(H)(η^3-$CH_2CHCHMe$) (**3a**).

Scheme 4. Reaction of 1 with PMe_3 at 60 °C

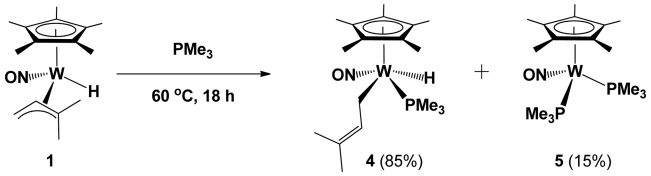

complexes **4** and **5** can be isolated together as an orange powder by slow recrystallization from pentane at −33 °C. However, various attempts to fully separate the two complexes have been unsuccessful in obtaining either in significant yield. For instance, both complexes decompose on a variety of column supports including basic and neutral alumina and silica, both in air and under an inert atmosphere. Large-scale fractional recrystallization is unsuccessful in separating the two complexes completely. Fortunately, a small sample of **4** can be isolated as large yellow crystals by slow evaporation of an Et_2O solution at −33 °C over 1 week, and the complete characterization of **4** has been effected with these crystals. Interestingly, the formation of **4** is reversible under ambient conditions. Thus, monitoring of a C_6D_6 solution of pure **4** by ^1H and ^{31}P NMR spectroscopy over several weeks reveals the growth of signals due to **1** and free PMe_3 and the consumption of **4**. After approximately 2.5 weeks, signals due to **4** are no longer evident. The reversibility of the formation of **4** explains, in part, the difficulty separating the mixture of **4** and **5** in an appreciable quantity. Consistently, if the thermal reaction of **1** is not carried out in neat PMe_3, the conversion of **1** to **4** never reaches 100% completion.

Complexes **4** and **5** each exist as a single coordination isomer in solution. The $^{31}P\{^1H\}$ NMR spectrum of the mixture of **4** and **5** in C_6D_6 is shown in Figure 7. The signal due to the

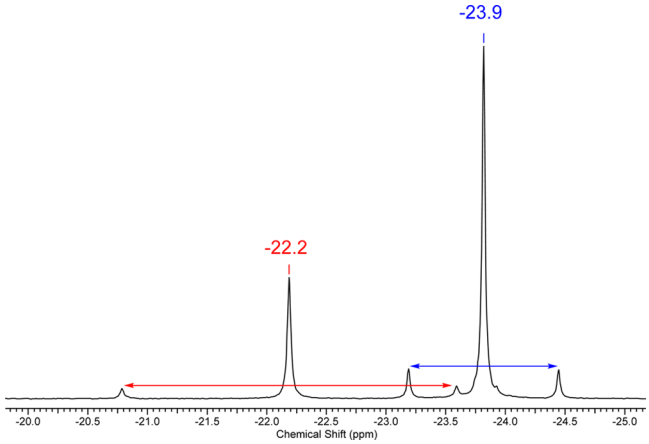

Figure 7. Expansion of the $^{31}P\{^1H\}$ NMR spectrum (−21.8 to −25.2 ppm) of the mixture of **4** and **5** in C_6D_6 (162 MHz) displaying the resonances due to the W*P*Me_3 phosphorus nuclei of **4** (δ −23.9, $^1J_{PW}$ = 204.1 Hz) and **5** (δ −22.2, $^1J_{PW}$ = 456.8 Hz).

phosphorus atom of **4** at δ −23.9 ppm is a singlet with tungsten-183 satellites having $^1J_{WP}$ = 204.1 Hz. The resonance due to the two equivalent phosphorus atoms of **5** at δ −22.2 ppm has a much larger $^1J_{PW}$ coupling of 456.8 Hz.

The nitrosyl-stretching frequency in the infrared spectrum of **4** at 1563 cm^{-1} indicates a weaker NO bond and a greater degree of tungsten−nitrosyl backbonding than in the precursor complex **1**, which has a ν_{NO} of 1601 cm^{-1}. This feature is the result of the strongly Lewis basic PMe_3 ligand donating electron density to the metal center in **4**. Consistently, in the case of **5**, which possesses two PMe_3 ligands, the nitrosyl-stretching frequency is even lower (ν_{NO} = 1552 cm^{-1}).

The solid-state molecular structure of **4** is shown in Figure 8. It is an 18e four-legged piano-stool molecule with only a single

DOI: 10.1021/acs.inorgchem.5b00747
Inorg. Chem. 2015, 54, 5915−5929

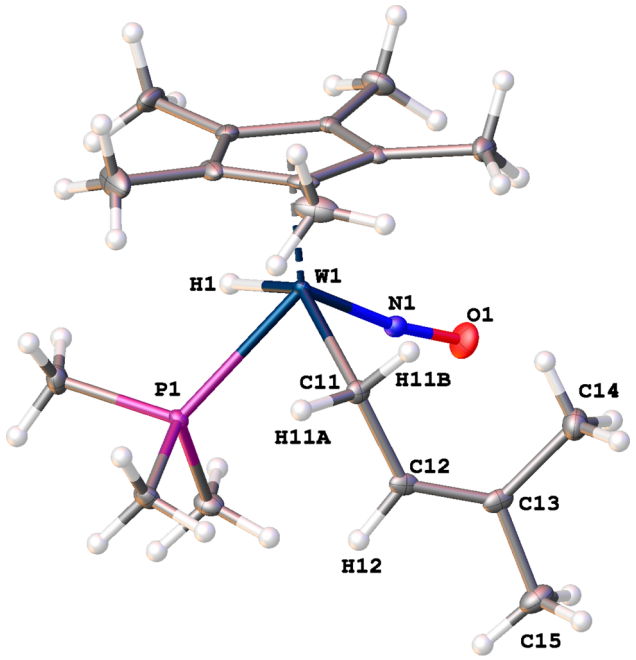

Figure 8. Solid-state molecular structure of **4** with 50% probability thermal ellipsoids shown. Selected bond lengths (Å) and angles (deg): W(1)−H(1) = 1.64(3), W(1)−P(1) = 2.4913(9), W(1)−C(11) = 2.259(2), C(11)−C(12) = 1.492(3), C(12)−C(13) = 1.339(3), C(11)−H(11A) = 1.06(3), C(11)−H(11B) = 0.99(3), C(12)−H(12) = 1.00(3), W(1)−N(1) = 1.784(2), N(1)−O(1) = 1.224(2), C(11)−C(12)−C(13) = 127.7(2), C(12)−C(13)−C(14) = 123.7(2), C(12)−C(13)−C(15) = 122.4(2), W(1)−N(1)−O(1) = 171.87(16).

coordination isomer containing the PMe_3 ligand *trans* to the nitrosyl and *cis* to both the hydride and the η^1-allyl ligands. The *trans* orientation of the PMe_3 and nitrosyl ligands is likely a manifestation of the strong σ-donor ability of the phosphine ligand and the strong π-acceptor character of the nitrosyl ligand. The hydride ligand has been located in the electron-density map, and the W−H bond length (1.64(3) Å) is essentially the same as that found for complex **1** (1.62(3) Å). The C(11)−C(12) and C(12)−C(13) bond lengths are indicative of single C−C and double C═C bonds with lengths of 1.492(3) and 1.339(3) Å, respectively, and the bond angles containing C(12) and C(13) are all consistent with the presence of sp^2-hybridized C atoms.

In the ^{1}H and ^{13}C NMR spectra of **4**, resonances due to the hydride and η^1-allyl ligands *trans* to the phosphine show scalar coupling to the phosphorus atom through the tungsten center. The resonance due to the tungsten hydride in the ^{1}H NMR spectrum of **4** is very distinct and appears as a doublet of triplets with tungsten-183 satellites. The overlaid ^{1}H and ^{1}H{^{31}P} NMR spectra of **4** are shown in Figure 9. The hydride resonance is coupled to the phosphorus atom of the WPMe_3 through the metal center ($^2J_{PH}$ = 81.2 Hz), the tungsten center ($^1J_{WH}$ = 61.8 Hz), and the two methylene protons of the η^1-CH_2CH═CMe_2 ligand ($^3J_{HH}$ = 4.1 Hz) adjacent to the tungsten. The methylene and methine carbon atoms of the η^1-allyl ligand both show coupling to the PMe_3 phosphorus atom in the ^{13}C NMR spectrum. The resonance at 16.4 ppm due to η^1-CH_2CH═CMe_2, C(11), shows coupling to both the phosphorus ($^2J_{PC}$ = 14.2 Hz) and tungsten ($^1J_{WC}$ = 63.5 Hz) atoms; this feature confirms the point of attachment of the η^1-allyl ligand to the tungsten and is consistent with the solid-state

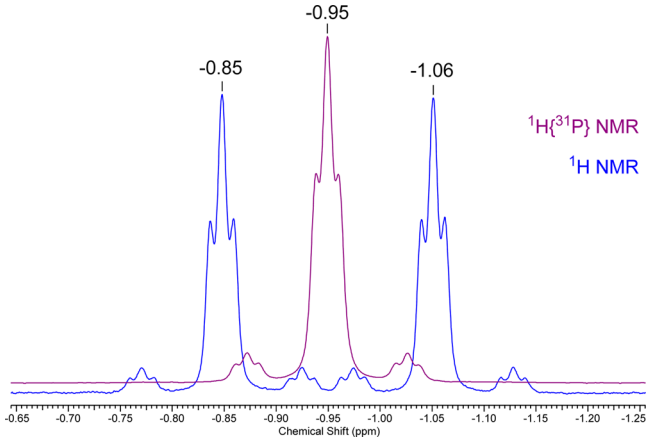

Figure 9. Expansion of the overlaid ^{1}H (blue) and ^{1}H{^{31}P} (purple) NMR spectra (−0.65 to −0.1.25 ppm) of **4** in C_6D_6 (400 MHz) displaying the resonances due to the W*H* proton of **4** (δ −0.95, $^3J_{HH}$ = 4.3, $^2J_{PH}$ = 81.4, $^1J_{WH}$ = 61.8 Hz).

molecular structure. The signal at 135.6 ppm due to the η^1-CH_2CH═CMe_2 also shows coupling to the phosphorus ($^3J_{PC}$ = 8.3 Hz), albeit with a slightly smaller magnitude, consistent with the larger distance between the atoms. The strong coupling of the phosphorus atom of the PMe_3 ligand with H and C atoms on ligands oriented *cis* to it is also evident in the NMR spectra of complex **7** (vide infra) and can be used to assign the position of a ligand *cis* or *trans* relative to PMe_3 for compounds whose Sel NOE and/or NOESY spectra are not sufficient to assign isomers, such as in the cases of multiple coordination isomers possessing many overlapping signals in their ^{1}H NMR spectra.

The thermolysis of **2** at 60 °C in neat PMe_3 for 18 h affords the three organometallic complexes Cp*W(NO)(H)(η^1-CH_2CH═$CHPh$)(PMe_3) (**6**), Cp*W(NO)(η^2-MeCH═CHPh)(PMe_3) (**7**), and **5** in a 41:48:11 ratio (Scheme 5). This mixture can be fractionally recrystallized from Et_2O at −33 °C to obtain red (**5**) and yellow (**6**, **7**) crystals. Quantitative separation of the mixture has not been achieved due to the instability of the complexes on various chromatographic columns, but a sufficient quantity of crystals could be separated to allow for the full characterization of **6** and **7**.

Complex **6** is analogous to **4** (vide supra) in that the PMe_3 coordinates to the tungsten center *trans* to the nitrosyl ligand and the allyl ligand is shifted to an η^1 coordination mode. The solid-state molecular structure of **6** is shown in Figure 10. There are two asymmetric molecules in the unit cell, both belonging to a single coordination isomer of **6**. The hydride ligand could not be located in the electron-density map generated by X-ray diffraction for either asymmetric unit. However, an open coordination site that could accommodate it exists for each molecule *trans* to the η^1-allyl ligand and *cis* to the nitrosyl and PMe_3 ligands which are oriented *trans* to each other. This four-legged piano-stool geometry of the molecule closely resembles that of complex **4**. Thus, the bond lengths and angles about the C(11)−C(12) and C(33)−C(34) are consistent with C═C double bonds and sp^2-hybridized C atoms. The characteristic W*H* signal in the ^{1}H NMR spectrum is also analogous to that of **4**, with a chemical shift of −0.62 ppm and scalar coupling to the tungsten, and *cis* oriented PMe_3 and η^1-CH_2CH═$CHPh$ ligands ($^2J_{HP}$ = 80.6, $^1J_{WH}$ = 30.6, $^3J_{HH}$ = 4.3 Hz).

DOI: 10.1021/acs.inorgchem.5b00747
Inorg. Chem. 2015, 54, 5915−5929

Scheme 5. Reaction of 2 with PMe_3 at 60 °C

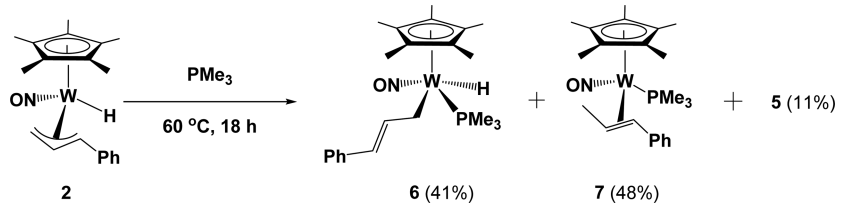

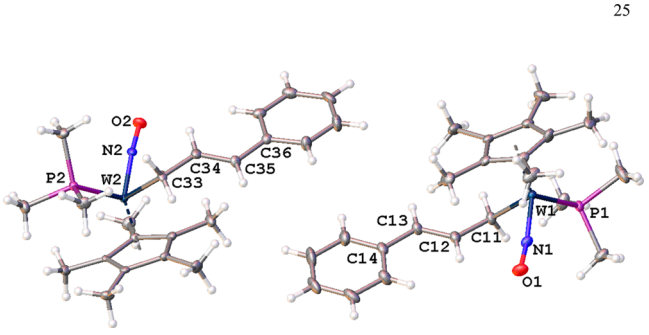

Figure 10. Solid-state molecular structure of **6** with 50% probability thermal ellipsoids shown. Selected bond lengths (Å) and angles (deg): W(1)−P(1) = 2.4951(10), W(1)−C(11) = 2.284(4), C(11)−C(12) = 1.482(5), C(12)−C(13) = 1.339(5), C(13)−C(14) = 1.466(5), W(1)−N(1) = 1.785(3), N(1)−O(1) = 1.223(4), C(11)−C(12)−C(13) = 127.5(4), C(12)−C(13)−C(14) = 125.5(4), W(1)−N(1)−O(1) = 168.8(3), W(2)−P(2) = 2.4910(10), W(2)−C(33) = 2.302(4), C(33)−C(34) = 1.480(5), C(34)−C(35) = 1.346(5), C(35)−C(36) = 1.468(5), W(2)−N(2) = 1.792(3), N(2)−O(2) = 1.224(4), C(33)−C(34)−C(35) = 129.1(4), C(34)−C(35)−C(36) = 124.5(4), W(2)−N(2)−O(2) = 171.6(3).

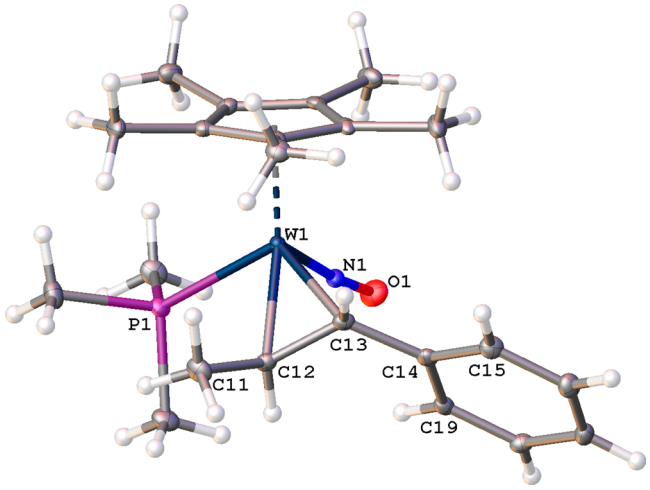

Figure 11. Solid-state molecular structure of **7** with 50% probability thermal ellipsoids shown. Selected bond lengths (Å) and angles (deg): W(1)−P(1) = 2.4535(10), W(1)−C(12) = 2.232(3), W(1)−C(13) = 2.216(3), C(11)−C(12) = 1.520(4), C(12)−C(13) = 1.449(4), C(13)−C(14) = 1.488(4), C(12)−H(12) = 0.98(4), C(13)−H(13) = 0.93(4), W(1)−N(1) = 1.781(3), N(1)−O(1) = 1.227(4), C(11)−C(12)−C(13) = 118.5(3), C(12)−C(13)−C(14) = 123.4(3), W(1)−N(1)−O(1) = 172.8(2).

The other new compound formed from the reaction of **2** with PMe_3 is complex **7**, which is the result of the coupling of the hydride and allyl ligands to generate a 16e η^2-alkene complex, Cp*W(NO)(η^2-MeCH═CHPh), to which a PMe_3 molecule has coordinated. Large yellow crystals of **7** suitable for a single-crystal X-ray diffraction analysis can be grown by slow evaporation from Et_2O at room temperature. There is only a single coordination isomer of **7** both in solution and in the solid state. The η^2-coordination mode of the *trans*-β-methylstyrene ligand is clearly evident in the solid-state molecular structure shown in Figure 11. The C(11)−C(12) bond length of 1.449(4) Å is significantly elongated compared to a typical C═C double bond. Additionally, despite having a C═C bond adjacent to the phenyl ring, the ligand is not planar, but significantly distorted, having a C(12)−C(13)−C(14)−C(19) torsion angle of 34.2(4)°. Both of these features indicate a considerable degree of tungsten-to-ligand backbonding. This bonding is intermediate between that of an η^2-alkene complex and a three-membered metallacyclopropane, with the C−C bond length as well as the bond angles containing C(12) and C(13) being in between typical sp^2- and sp^3-hybridized C atoms. The ^{1}H NMR spectrum of **7** is also consistent with a significant tungsten interaction with the bound-olefin ligand, the signals due to the two alkene protons being significantly shifted upfield relative to a free alkene at 2.48 and 2.04 ppm.

The orientation of the methyl substituent *cis* to the PMe_3 ligand is evident in the solid-state molecular structure and is further confirmed by phosphorus coupling in the ^{1}H and ^{13}C NMR spectra of **7** (Figure 12a.). ^{1}H−^{31}P coupling can be observed through tungsten and carbon bonds, as shown in

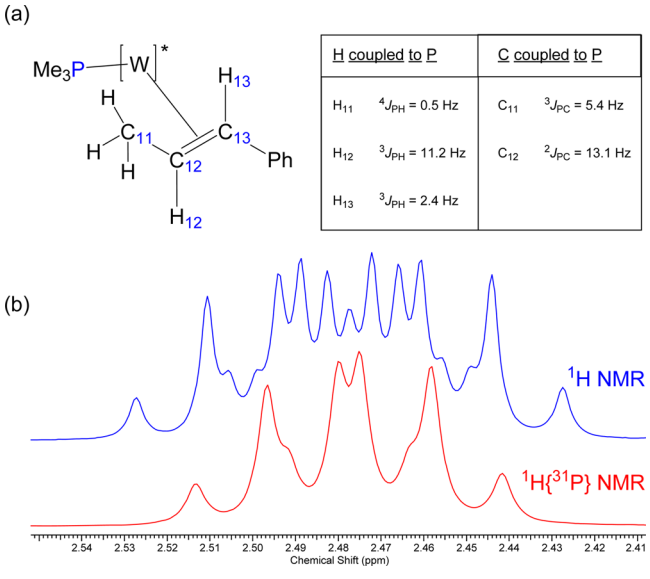

Figure 12. (a) Diagram displaying the ^{31}P coupling to the η^2-alkene ^{1}H and ^{13}C signals. (b) Expansion of the overlaid ^{1}H (blue) and ^{1}H{^{31}P} (purple) NMR spectra (2.55−2.41 ppm) of **7** in C_6D_6 (400 MHz) displaying the resonances (ddq) due to the *Me*CH═CHPh proton of **7** (δ −2.48, $^3J_{PH}$ = 11.2, $^3J_{HH}$ = 8.8, 6.6 Hz).

Figure 12b, in which the signal due to MeC*H*CHPh displays coupling to the adjacent methyl ($^3J_{HH}$ = 6.6 Hz) and methine

DOI: 10.1021/acs.inorgchem.5b00747
Inorg. Chem. 2015, 54, 5915−5929

Scheme 6. Reaction of 1 with PMe_3 at 80 °C

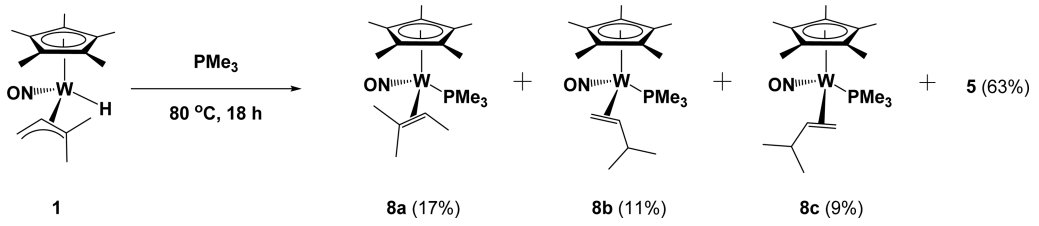

1 **8a** (17%) **8b** (11%) **8c** (9%)

($^3J_{HH}$ = 8.8 Hz) protons as well as PMe_3 ($^3J_{PH}$ = 11.2 Hz). The signals due to the alkene methyl and methine protons all display phosphorus−proton coupling; the C*H cis* to the PMe_3 has a larger $^3J_{PH}$ than the C*H* located *trans* to the PMe_3 ligand (11.2 Hz vs 2.4 Hz). Likewise, the resonances due to the carbon CH and *Me* atoms located *cis* to the PMe_3 ligand are the only C atoms that display any $^{13}C-^{31}P$ coupling. The $^1H-^{31}P$ and $^{13}C-^{31}P$ couplings in the ^1H and ^{13}C NMR spectra, respectively, occur predominantly with ligands or parts of ligands located *cis* to the PMe_3 ligand; this *cis* P coupling is also observed for complex **4** (vide supra). Therefore, the correlation made from the X-ray solid-state molecular structures and NMR spectroscopy is that phosphorus coupling through the tungsten center occurs with ligands *cis* to the PMe_3. This fact is important for structural assignments of complexes for which single crystals suitable for X-ray diffraction cannot be obtained and complexes having several coordination isomers with many overlapping signals that make solution-structure determinations using Sel NOE and NOESY NMR spectroscopy unreliable. This aspect has also been used for the assignment of the orientation of the η^2-alkene ligands in the coordination isomers of complexes **8** and **9** (vide infra).

In contrast with the reaction of **2** with PMe_3 that produces both the η^1-allyl hydrido and η^2-alkene PMe_3 adducts (Scheme 5), there is no evidence for an analogue of **7** in the final reaction mixture involving **1** under the same conditions. The reaction of **1** with neat PMe_3 carried out at a higher temperature (80 °C) results in the formation of **5** and the PMe_3-trapped η^2-alkene complexes, Cp*W(NO)(η^2-MeCH═CMe$_2$)(PMe_3) (**8a**) and Cp*W(NO)(η^2-CH$_2$═CHCHMe$_2$)(PMe_3) (**8b**, **8c**) (Scheme 6). Complex **5** is formed as the major component of the reaction mixture, and the isomers of **8** cannot be separated from **5** by fractional recrystallization or column chromatography, the latter resulting in decomposition of all of the organometallic products. The similar and overlapping signals in the ^1H and ^{13}C NMR spectra due to the three isomers of **8** preclude establishment of the exact orientations of their η^2-alkene ligands via NOESY NMR spectroscopy. The orientations indicated in Scheme 6 are thus based on the $^1H-^{31}P$ and $^{13}C-^{31}P$ scalar couplings in the ^1H and ^{13}C NMR spectra, respectively. The $^{31}P\{^1H\}$ NMR spectrum involving the three isomers of **8** is shown in Figure 13. The three isomers all possess similar chemical shifts (δ −11.1 to −15.2 ppm) and $^1J_{WP}$ frequencies (358−373 Hz). These values are in the range typical for Cp*W(NO)(η^2-C═C)(PMe_3) complexes (vide infra).

The thermolysis of **3** in neat PMe_3 at 60 °C produces coordination isomers of the trapped 16e η^2-alkene complexes, Cp*W(NO)(η^2-CH$_2$═CHCH$_2$Me)(PMe_3) (**9a**, **9b**, **9d**) and Cp*W(NO)(η^2-MeCH═CHMe)(PMe_3) (**9c**), and complex **5** in a 41:26:25:5:3 ratio (Scheme 7). While crystals suitable for single-crystal X-ray diffraction analyses have not been obtained, the coordination of the alkene C═C bond to the tungsten

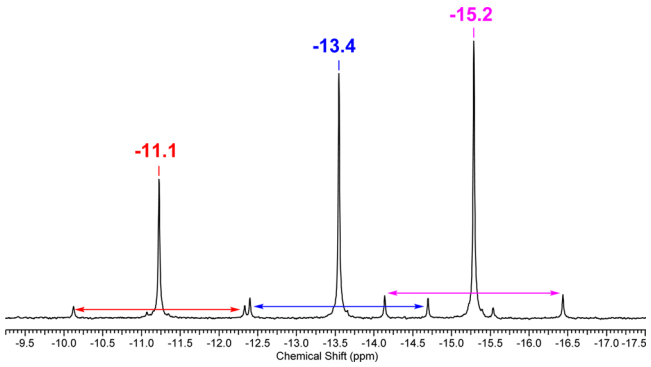

Figure 13. Expansion of the $^{31}P\{^1H\}$ NMR spectrum (−9.3 to −17.5 ppm) of **8** in C_6D_6 (162 MHz) displaying the resonances due to the W*P*Me$_3$ phosphorus nuclei of **8a** (δ −15.2, $^1J_{PW}$ = 373 Hz), **8b** (δ −13.4, $^1J_{PW}$ = 372 Hz), and **8c** (δ −11.1, $^1J_{PW}$ = 358 Hz).

center has been established for each isomer via ^{183}W satellites on the alkene signals in the ^{13}C NMR spectrum. Phosphorus-31 coupling in the ^1H and ^{13}C NMR spectra has again been used to assign the orientation of the alkene ligands, with the ^{13}C and ^1H atoms whose signals display ^{31}P-coupling being *cis* to the PMe_3 ligand. The expansion of the $^{31}P\{^1H\}$ NMR spectrum displaying the resonances due to *P*Me$_3$ ligands for the isomers of **9** is shown in Figure 14. The chemical shift and $^1J_{WP}$ values are consistent with the similar η^2-alkene adducts discussed previously (vide supra).

Attempts to isolate the Cp*W(NO)(H)(η^1-CH$_2$CH═CHMe)(PMe_3) complex (**10**) that is analogous to **4** and **6** in significant quantity from the reaction of **3** with PMe_3 have been unsuccessful. It can be detected spectroscopically by its characteristic W*H* signal in the ^1H NMR spectrum [δ −0.81 (dt, $^3J_{HH}$ = 4.6, $^2J_{PH}$ = 80.2 Hz, $^1J_{WH}$ = 62.0 Hz, 1H)] and W*P*Me$_3$ signal in the $^{31}P\{^1H\}$ NMR spectrum [δ −24.0 (s, $^1J_{PW}$ = 203.6 Hz)], both of which are similar to the corresponding signals displayed by **4** and **6** in terms of chemical shifts and coupling constants. The reaction mixture in which **10** can be detected contains mainly isomers of **9** as well as some unreacted **3**. This observation suggests that complex **10** is unstable under the conditions required to form it and is largely converted to **9** before the starting complex has been completely consumed.

EPILOGUE

This study has demonstrated that the strong coupling of the phosphorus atom of the PMe_3 ligand with H and C atoms on ligands oriented *cis* to it can be used to establish whether a ligand is *cis* or *trans* to PMe_3 in the metal's coordination sphere and is particularly useful for compounds whose Sel NOE and/or NOESY spectra do not provide a definitive answer. Furthermore, the current investigations have also demonstrated that the 18e Cp*W(NO)(H)(η^3-allyl) compounds can undergo

DOI: 10.1021/acs.inorgchem.5b00747
Inorg. Chem. 2015, 54, 5915−5929

Scheme 7. Reaction of 3 with PMe_3 at 60 °C

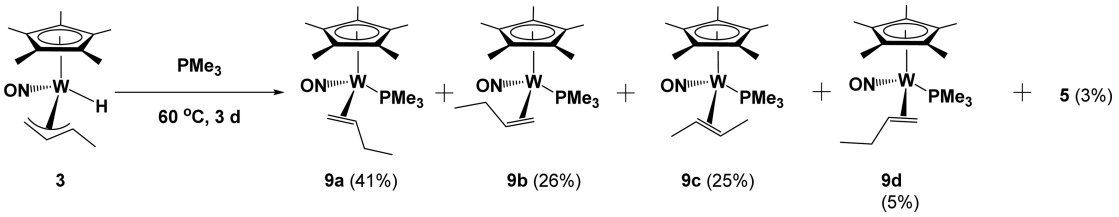

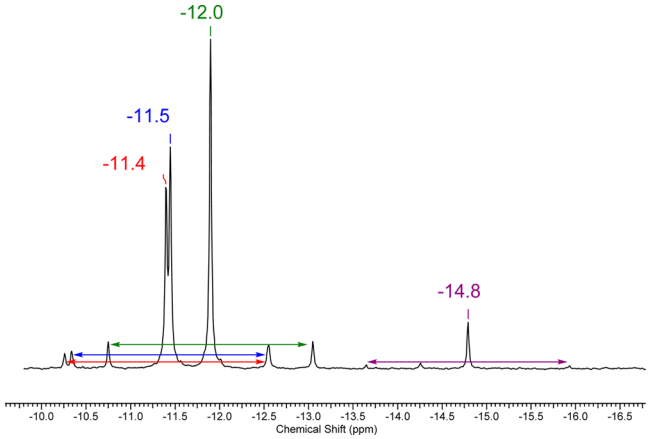

Figure 14. Expansion of the $^{31}P\{^1H\}$ NMR spectrum (−9.6 to −16.7 ppm) of **9** in C_6D_6 (162 MHz) displaying the resonances due to the $WPMe_3$ phosphorus nuclei of **9a** (δ −12.0, $^1J_{PW}$ = 372.6 Hz), **9b** (δ −11.5, $^1J_{PW}$ = 358.7 Hz), **9c** (δ −11.4, $^1J_{PW}$ = 369.9 Hz), and **9d** (δ −14.8 ($^1J_{WP}$ = 370.6 Hz).

intramolecular isomerizations upon thermolysis to the corresponding 16e Cp*W(NO)(η^2-alkene) complexes. The intriguing question that immediately comes to mind is whether these intermediate alkene species can effect the intermolecular activations of hydrocarbon C−H bonds and, if so, how do these activations compare with those documented for the related 16e Cp*W(NO)(η^2-allene) and Cp*W(NO)(η^2-diene) entities. We have initiated investigations to provide answers to these questions, and we shall be reporting the results of our ongoing studies in due course.

EXPERIMENTAL SECTION

General Methods. All reactions and subsequent manipulations involving organometallic reagents were performed under anhydrous and anaerobic conditions except where noted. All inert gases were purified by passing them through a column containing MnO and then through a column of activated 4 Å molecular sieves. High vacuum and inert atmosphere techniques were performed either using double-manifold Schlenk lines or in Innovative Technologies LabMaster 100 and MS-130 BG dual-station gloveboxes equipped with freezers maintained at −33 °C. Preparative scale reactions were performed with Schlenk or round-bottom flasks; reactions were performed in thick-walled glass reaction bombs (larger scale) or J. Young NMR tubes (smaller scale), both of which were sealed by Kontes greaseless stopcocks. Tetrahydrofuran (THF) was dried over sodium/benzophenone ketyl and freshly distilled prior to use; solvents such as pentane, hexanes, and diethyl ether (Et_2O) were not dried prior to use. All other solvents were dried according to standard procedures.[7] All binary magnesium reagents used were prepared from the corresponding Grignard reagents.[8] The complex Cp*W(NO)Cl_2 was prepared according to the published procedures.[9] Pentamethylcyclopentadiene was obtained from the Boulder Scientific Company, and $LiBH_4$ (2.0 M in MeTHF) was obtained from Sigma-Aldrich. All other chemicals and reagents were ordered from commercial suppliers and used as received.

Unless otherwise specified, all IR samples were prepared as Nujol mulls sandwiched between NaCl plates, and their spectra were recorded on a Thermo Nicolet model 4700 FT-IR spectrometer. Except where noted, all NMR spectra were recorded at room temperature on Bruker AV-300, AV-400 (direct and indirect probes), and AV-600 instruments, and all chemical shifts are reported in ppm and coupling constants are reported in Hz. ^1H NMR spectra were referenced to the residual protio isotopomer present in C_6D_6 (7.16 ppm). ^{13}C NMR spectra were referenced to C_6D_6 (128.39 ppm). ^{31}P NMR spectra were externally referenced to 85% H_3PO_4. For the characterization of most complexes, two-dimentional NMR experiments, $\{^1H-^1H\}$ COSY,$\{^1H-^{13}C\}$ HSQC, and $\{^1H-^{13}C\}$ HMBC, were performed to correlate and assign ^1H and ^{13}C NMR signals and establish atom connectivity; ^1H NOE NMR and $\{^1H-^1H\}$ NOESY were used for determination of solution structures. Low-resolution mass spectra (EI, 70 eV) were recorded by Mr. Marshall Lapawa of the UBC mass spectrometry facility using a Kratos MS-50 spectrometer, and elemental analyses were performed by Mr. Derek Smith of the UBC microanalytical facility. X-ray crystallographic data collection, solution, and refinement were performed at the UBC X-ray crystallography facility.

Preparation of Cp*W(NO)(H)(η^3-CH_2CHCMe_2) (1a, 1b). In a glovebox, a glass Schlenk flask was charged with Cp*W(NO)Cl_2 (5.14 g, 12.2 mmol), THF (ca. 150 mL), and a magnetic stir bar, and it was then cooled in a dry ice/acetone bath (−78 °C). A second Schlenk flask was charged with $Mg(CH_2CH{=}CMe_2)_2$ (1.57 g, 12.3 mmol, 128 g/mol titer) and THF (ca. 100 mL), and then the contents were transferred to the first flask dropwise via cannula. Following this addition, the reaction mixture was allowed to warm to room temperature and was then stirred for 1 h to obtain a yellow-brown mixture. The Schlenk flask was again cooled to −78 °C, and 2 equiv of $LiBH_4$ (12.0 mL, 24 mmol, 2.0 M in THF) was added slowly via syringe. The contents of the Schlenk flask were warmed to room temperature and stirred for 3 h to obtain a brown mixture. The THF solvent was removed in vacuo, and the resulting residue was dissolved in Et_2O (ca. 100 mL) and washed with H_2O (3 × 50 mL). The Et_2O layer was filtered through a glass frit, the filtrate was collected in a Schlenk flask, and then the solvent volume was reduced in vacuo to obtain a concentrated solution of the crude mixture. Purification was performed by column chromatography using a neutral alumina support. A yellow band was eluted with 0−35% Et_2O in hexanes. The solvent was removed from the eluate under reduced pressure to obtain Cp*W(NO)(H)(η^3-CH_2CHCMe_2) (**1**) as a yellow powder (2.30 g, 45% yield). Pale yellow rod-shaped crystals of **1** suitable for a single-crystal X-ray diffraction analysis were grown from Et_2O at −33 °C. Two isomers of the complex, **1a** and **1b**, were identified in solution by ^1H NMR spectroscopy in a 83:17 ratio, respectively. The solution molecular structure was elucidated by Sel NOE and NOESY NMR spectroscopy. The melting point of **1** was recorded as 123−125 °C and is reversible since the presence of **1** was confirmed by ^1H NMR spectroscopy following the melt.

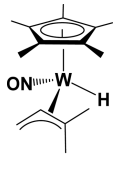

1a (83%)

DOI: 10.1021/acs.inorgchem.5b00747
Inorg. Chem. 2015, 54, 5915−5929

Characterization data for **1a** (83%): IR (cm^{-1}): 1601 (s, ν_{NO}). MS (LREI, *m/z*, probe temperature 120 °C): 419 [M^+, ^{184}W]. ^1H NMR (600 MHz, C_6D_6): δ −0.90 (s, $^1J_{WH}$ = 127.9, 1H, W*H*), 1.72 (s, 15H C_5Me_5), 1.90 (s, 3H, allyl *Me*), 2.06 (m, 1H, allyl CH_2), 2.29 (s, 3H, allyl *Me*), 2.42 (dd, $^3J_{HH}$ = 13.1, $^2J_{HH}$ = 3.2, 1H, allyl CH_2), 2.68 (dd, $^3J_{HH}$ = 13.2, 7.7, 1H, allyl C*H*). ^{13}C APT NMR (150 MHz, C_6D_6): δ 11.03 (C_5Me_5), 25.0 (allyl *Me*), 30.7 (allyl *Me*), 37.6 (allyl CH_2), 96.0 (allyl CH), 100.3 (allyl CMe_2), 104.4 (C_5Me_5). Sel NOE (400 MHz, C_6D_6): δ irrad. at −0.90, NOE at 1.72, 1.90, 2.29. mp 123−125 °C (reversible, confirmed by ^1H NMR). Anal. Calcd for $C_{20}H_{25}NOW$: C, 42.98; H, 6.01; N, 3.34. Found: C, 42.85; H, 6.02; N, 3.27.

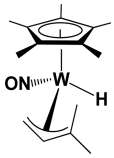

1b (17%)

Characterization data for **1b** (17%): ^1H NMR (600 MHz, C_6D_6): δ −0.59 (s, $^1J_{WH}$ = 127.4, 1H, W*H*), 0.56 (dd, $^3J_{HH}$ = 11.7, $^2J_{HH}$ = 3.8, 1H, allyl CH_2), 0.87 (s, 3H allyl *Me*), 1.74 (s, 15H C_5Me_5), 2.45 (s, 3H, allyl *Me*), 2.82 (m, 1H, allyl CH_2), 4.71 (dd, $^3J_{HH}$ = 11.7, 7.3, 1H, allyl C*H*). ^{13}C APT NMR (150 MHz, C_6D_6): δ 11.00 (C_5Me_5), 21.7 (allyl *Me*), 31.2 (allyl *Me*), 40.9 (allyl CH_2), 95.0 (allyl CMe_2), 103.2 (allyl CH), 105.4 (C_5Me_5).

Preparation of Cp*W(NO)(H)(η^3-$CH_2CHCHPh$) (2a, 2b, 2c, 2d). In a glovebox, a Schlenk flask was charged with Cp*W(NO)Cl_2 (5.000 g, 11.90 mmol) and a magnetic stir bar. A second Schlenk flask was charged with Mg(CH_2CH═$CHPh)_2$ (titer: 218 g/mol, 2.592 g, 11.90 mmol) and a magnetic stir bar. On a Schlenk line under argon, dry THF (ca. 100 mL each) was cannulated into each Schlenk flask, and each mixture was stirred until all solid material had dissolved. Both Schlenk flasks were then placed into a dry ice/acetone bath (−78 °C) while stirring of their contents was maintained. Once cold, the contents of the second Schlenk flask were cannulated slowly into the first Schlenk flask. The resulting mixture was then removed from the cold bath and allowed to reach room temperature while being stirred for 1 h. The first Schlenk flask was then placed back into the dry ice/acetone bath, and its contents were cooled to −78 °C. A solution of $LiBH_4$ in THF (2.0 M, 6.5 mL, 13 mmol) was added to the Schlenk flask in a dropwise fashion. The mixture developed a strong red-brown color, and it was removed from the cold bath and allowed to reach room temperature while being stirred for 3 h. Removal of the THF in vacuo left behind a reddish-brown oily residue. On the benchtop, this residue was redissolved in Et_2O, and the mixture was then filtered through Celite supported on a porous frit to remove the magnesium salts. The ether filtrate was dark reddish-brown in color at this stage, and it was reduced in volume in vacuo to obtain a concentrated solution of the crude product. Purification was performed by chromatography utilizing a neutral alumina column (10 cm × 2.5 cm) prepared in hexanes. A yellow band was eluted from the column with a gradient of 0−50% Et_2O in hexanes to obtain a yellow eluate. Solvent removal from this solution in vacuo afforded Cp*W(NO)(H)(η^3-$CH_2CHCHPh$) (**2**) as a yellow powder (1.115 g, 20% yield). Complex **2** exists as four isomers in solution; the ratio of the isomers (**2a**:**2b**:**2c**:**2d**, 71:26:2:1 respectively) was established by ^1H NMR spectroscopy.

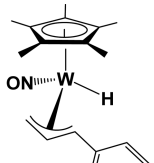

2a (71%)

Characterization data for **2a** (71%): IR (cm^{-1}): 1591 (s, ν_{NO}). MS (LREI, *m/z*, probe temperature 150 °C): 467 [M^+, ^{184}W]. ^1H NMR (400 MHz, C_6D_6): δ −0.49 (s, $^1J_{WH}$ = 120.4, 1H, W*H*), 0.42 (dt, $^3J_{HH}$ = 10.2, $^2J_{HH}$ = 1.2, 1H, allyl CH_2), 1.70 (s, 15H, C_5Me_5), 2.80 (d, $^3J_{HH}$ = 13.1, 1H, allyl C*H*Ph), 2.89 (dt, $^3J_{HH}$ = 7.1, $^2J_{HH}$ = 2.7, 1H, allyl CH_2), 5.36 (ddd, $^3J_{HH}$ = 13.1, 10.2, 7.1, 1H, allyl C*H*), 6.98 (t, $^3J_{HH}$ = 7.3, 1H, *p*-aryl *H*), 7.09−7.18 (m, 2H, *m*-aryl *H*), 7.25 (d, $^3J_{HH}$ = 8.0, 2H, *o*-aryl *H*). ^{13}C NMR (100 MHz, C_6D_6): δ 10.6 (C_5Me_5), 40.1 (allyl CH_2), 80.9 (allyl PhCH), 102.4 (allyl CH), 105.0 (C_5Me_5), 126.0 (*p*-aryl *C*), 126.5 (*o*-aryl *C*), 128.7 (*m*-aryl *C*), 142.4 (ipso *C*). Sel NOE (400 MHz, C_6D_6): δ irrad. at −0.49, NOE at 2.80, 7.25. mp 99−100 °C (reversible, confirmed by ^1H NMR). Anal. Calcd for $C_{19}H_{25}NOW$: C, 48.84; H, 5.39; N, 3.00. Found: C, 49.14; H, 5.30; N, 2.91.

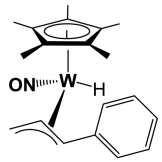

2b (26%)

Characterization data for **2b** (26%): ^1H NMR (400 MHz, C_6D_6): δ −0.34 (s, $^1J_{WH}$ = 126.4, 1H, W*H*), 1.63 (s, 15H, C_5Me_5), 2.28 (dt, $^3J_{HH}$ = 8.2, $^2J_{HH}$ = 2.6, 1H, allyl CH_2), 2.63 (dt, $^3J_{HH}$ = 12.4, $^2J_{HH}$ = 1.0, 1H, allyl CH_2), 3.76 (ddd, $^3J_{HH}$ = 14.1, 12.4, 8.0, 1H, allyl C*H*), 4.66 (d, $^3J_{HH}$ = 14.1, 1H, allyl C*H*Ph), 7.07 (obscured, 1H, *p*-aryl *H*), 7.13 (obscured, 2H, *m*-aryl *H*), 7.29 (obscured, 2H, *o*-aryl *H*). ^{13}C NMR (100 MHz, C_6D_6): δ 10.5 (C_5Me_5), 41.2 (allyl CH_2), 76.1 (allyl PhCH), 95.1 (allyl CH), 104.2 (C_5Me_5), obscured (*p*-aryl *C*), 126.8 (*o*-aryl *C*), obscured (*m*-aryl *C*), obscured (ipso *C*). Sel NOE (400 MHz, C_6D_6): δ irrad. at −0.34, NOE at 4.66, 7.13.

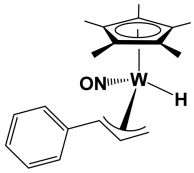

2c (2%)

Characterization data for **2c** (2%): ^1H NMR (400 MHz, C_6D_6): δ −0.87 (s, $^1J_{WH}$ = 128.6, 1H, W*H*), 0.77 (dt, $^3J_{HH}$ = 13.3, $^2J_{HH}$ = 1.0, 1H, allyl CH_2), 1.65 (s, 15H, C_5Me_5), 1.94 (d, $^3J_{HH}$ = 10.6, 1H, allyl C*H*Ph), 4.02 (dt, $^3J_{HH}$ = 7.1, $^2J_{HH}$ = 1.7, 1H, allyl CH_2), 5.03 (ddd, $^3J_{HH}$ = 13.2, 10.4, 7.1, 1H, allyl C*H*), 7.07 (t, $^3J_{HH}$ = 7.2, 1H, *p*-aryl *H*), 7.27 (t, $^3J_{HH}$ = 8.0, 2H, *m*-aryl *H*), 7.43 (d, $^3J_{HH}$ = 7.9, 2H, *o*-aryl *H*). ^{13}C APT NMR (100 MHz, C_6D_6): δ 10.4 (C_5Me_5), 50.6 (allyl CH_2), 66.9 (allyl PhCH), 103.5 (allyl CH), 104.8 (C_5Me_5), 125.5 (*p*-aryl *C*), 127.0 (*o*-aryl *C*), 128.7 (*m*-aryl *C*), obscured (ipso *C*). Sel NOE (400 MHz, C_6D_6): δ irrad. at −0.87, NOE at 0.77, 4.02.

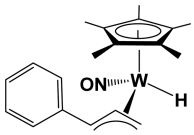

2d (1%)

Characterization data for **2d** (1%): ^1H NMR (400 MHz, C_6D_6): δ (selected signals) −0.69 (s, 1H, W*H*), 1.60 (s, 15H, C_5Me_5), 0.61 (dt, $^3J_{HH}$ = 13.1, $^2J_{HH}$ = 2.2, 1H, allyl CH_2), 4.11 (dt, $^3J_{HH}$ = 7.7, $^2J_{HH}$ = 2.1, 1H, allyl CH_2), 4.33 (ddd, $^3J_{HH}$ = 13.1, 10.1, 7.2, 1H, allyl C*H*). ^{13}C APT NMR (100 MHz, C_6D_6): δ (selected signals) 10.2 (C_5Me_5).

Preparation of Cp*W(NO)(H)(η^3-$CH_2CHCHMe$) (3a, 3b, 3c, 3d). In a glovebox, a Schlenk flask was charged with Cp*W(NO)Cl_2 (2.448 g, 5.827 mmol) and a magnetic stir bar. A second Schlenk flask was charged with Mg(CH_2CH═$CHMe)_2$ (0.543 g, 5.826 mmol, 93.2 g/mol titer) and a magnetic stir bar. The flasks were then removed from the glovebox and attached to a Schlenk line under nitrogen gas. Dry THF (ca. 100 mL each) was then cannulated into each flask, and then the contents of each flask were stirred to ensure complete dissolution of the solids. The Schlenk flask containing the Cp*W(NO)Cl_2 was then placed in a dry ice/acetone bath (−78 °C) while stirring of its contents continued. Once cold, the contents of the second flask were cannulated slowly into the first Schlenk flask quantitatively. The reaction flask was removed from the dry ice/

DOI: 10.1021/acs.inorgchem.5b00747
Inorg. Chem. 2015, 54, 5915−5929

acetone bath, and its contents were allowed to stir at room temperature for 1 h. Lithium borohydride in THF (2.0 M, 6.0 mL, 12 mmol) was added to the Schlenk flask in a dropwise fashion. The resulting mixture developed a slightly reddish brown color and was allowed to react at room temperature for 24 h. The volume of THF was reduced in vacuo, and water was added dropwise to the flask to neutralize the remaining $LiBH_4$. Liquid−liquid extractions with distilled water/Et_2O were carried out to remove salts from the mixture, and the organic layer was dried over anhydrous $MgSO_4$. The crude product was concentrated in vacuo and was purified by flash chromatography on neutral alumina. A yellow band was eluted with a gradient of 0−20% ethyl acetate in hexanes to obtain a bright yellow eluate. Solvent was removed from the eluate in vacuo to obtain Cp*W(NO)(H)(η^3-$CH_2CHCHMe$) as a dark yellow oil (0.455 g, 19% yield). X-ray-quality crystals of Cp*W(NO)(H)(η^3-$CH_2CHCHMe$) were obtained via slow evaporation of an Et_2O solution of the compound at room temperature. In solution, four coordination isomers of Cp*W(NO)(H)(η^3-$CH_2CHCHMe$) were identified by ^1H and ^{13}C NMR spectroscopy. The solution structures of the individual isomers were elucidated by ^1H Sel NOE NMR spectroscopy.

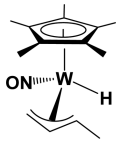

3a (67%)

Characterization data for **3a** (66.5%): IR (C_6D_6, cm^{-1}): 1571 (s, ν_{NO}). MS (LREI, *m/z*, probe temperature 120 °C): 405 [M^+, ^{184}W]. HRMS-EI *m/z*: [M^+, ^{186}W] Calcd for $C_{14}H_{23}NO^{186}W$ 407.13234. Found 407.13211. ^1H NMR (600 MHz, C_6D_6): δ −1.27 (s, $^1J_{WH}$ = 122.2, 1H, W*H*), 0.16 (d, $^3J_{HH}$ = 10.3, 1H, allyl CH_2), 1.74 (s, 15H C_5Me_5), 1.83 (m, 1H, allyl C*H*Me), 2.26 (d, $^3J_{HH}$ = 5.8, 3H, allyl *Me*), 2.75 (d, $^3J_{HH}$ = 7.3, 1H, allyl CH_2), 4.61 (ddd, $^3J_{HH}$ = 13.1, 10.3, 7.3, 1H, allyl C*H*). ^{13}C APT NMR (150 MHz, C_6D_6): δ 10.99 (C_5Me_5), 21.8 (allyl *Me*), 39.2 ($^1J_{WC}$ = 30.7, allyl CH_2), 78.6 (allyl *C*HMe), 104.6 (allyl CH), 105.0 (C_5Me_5). Sel NOE (600 MHz, C_6D_6): δ irrad. at −1.27, NOE at 2.26. mp 75−78 °C (reversible, confirmed by ^1H NMR). Anal. Calcd for $C_{14}H_{23}NOW$: C, 41.50; H, 5.72; N, 3.46. Found: C, 41.22; H, 5.71; N, 3.26.

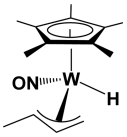

3b (17%)

Characterization data for **3b** (17.5%): ^1H NMR (600 MHz, C_6D_6): δ −1.33 (s, $^1J_{WH}$ = 122.6, 1H, W*H*), 0.59 (d, $^3J_{HH}$ = 13.5, 1H, allyl CH_2), 0.97 (dq, $^3J_{HH}$ = 10.0, 5.8, 1H, allyl C*H*Me), 1.72 (s, 15H C_5Me_5), 1.95 (d, $^3J_{HH}$ = 5.8, 3H, allyl *Me*), 4.08 (d, $^3J_{HH}$ = 7.3, 1H, allyl CH_2), 4.35 (ddd, $^3J_{HH}$ = 13.5, 10.0, 7.3, 1H, allyl C*H*). ^{13}C APT NMR (150 MHz, C_6D_6): δ 11.01 (C_5Me_5), 18.6 (allyl *Me*), 51.9 (allyl CH_2), 58.8 ($^1J_{WC}$ = 23.2, allyl *C*HMe), 104.8 (C_5Me_5), 104.9 (allyl CH). Sel NOE (600 MHz, C_6D_6): δ irrad. at −1.33, NOE at 4.09.

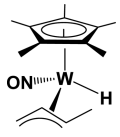

3c (14%)

Characterization data for **3c** (13.7%): ^1H NMR (600 MHz, C_6D_6): δ −1.24 (s, $^1J_{WH}$ = 124.3 1H, W*H*), 1.71 (s, 15H C_5Me_5), 2.06 (m, 1H, allyl CH_2), 2.14 (m, 3H, allyl *Me*), 2.28 (obscured, 1H, allyl CH_2), 2.82 (m, 1H, allyl C*H*), 3.65 (m, 1H, allyl C*H*Me). ^{13}C APT NMR (150 MHz, C_6D_6): δ 10.8 (C_5Me_5), 20.9 (allyl *Me*), 39.0 ($^1J_{WC}$ = 24.3, allyl CH_2), 74.9 (allyl CHMe), 99.1 (allyl CH), 104.2 (C_5Me_5).

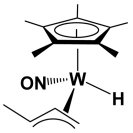

3d (2%)

Characterization data for **3d** (2.3%): ^1H NMR (600 MHz, C_6D_6): δ (selected signals) −0.86 (s, $^1J_{WH}$ = 124.8, 1H, W*H*), 1.69 (s, 15H C_5Me_5), 2.48 (m, 1H, allyl C*H*). ^{13}C APT NMR (150 MHz, C_6D_6): δ (selected signals) 10.9 (C_5Me_5), 94.1 (allyl CH), 104.3 (C_5Me_5).

Reaction of 1 with PMe_3. In a glovebox, a glass bomb was charged with **1** (0.432 g, 1.03 mmol), PMe_3 (ca. 7 mL), and a magnetic stir bar to obtain a golden-colored solution. The bomb was sealed with a Kontes greaseless stopcock and then placed into an oil bath. The contents of the bomb were heated at 60 °C while being stirred for 18 h, whereupon a red reaction mixture was obtained. The solvent was removed in vacuo, and an orange solid (0.376 g, combined yield of 74%) was obtained by recrystallization of the residue from pentane at −33 °C for 2 h. This solid contained a mixture of Cp*W(NO)(H)(η^1-$CH_2CH{=}CMe_2$)(PMe_3) (**4**) and Cp*W(NO)-(PMe_3)$_2$ (**5**) in a 85:15 ratio (by ^1H NMR spectroscopy). Several attempts to separate **4** and **5** were made. Column chromatography on basic alumina resulted in their partial separation, albeit with the formation of several new products that were recovered with **4**. Column chromatography on neutral alumina led to the decomposition of both products, while column chromatography on silica did lead to separation, but only small amounts of the products were recovered. Large yellow crystals that were suitable for X-ray diffraction were grown by dissolving the solid in Et_2O (ca. 1 mL), adding a layer of pentane (ca. 1 mL), and letting the mixture sit undisturbed for 1 week at −33 °C.

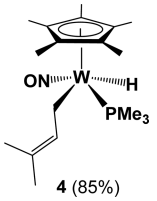

4 (85%)

Characterization data for **4** (85%): IR (cm^{-1}): 1563 (s, ν_{NO}), MS (LREI, *m/z*, probe temperature 150 °C): 495 [M^+, ^{184}W]. ^1H NMR (400 MHz, C_6D_6): δ −0.95 (dt, $^3J_{HH}$ = 4.3, $^2J_{PH}$ = 81.4, $^1J_{WH}$ = 61.8, 1H, W*H*), 1.11 (d, $^2J_{PH}$ = 8.4, 9H), 1.52 (m, 1H, CH_2CH=CMe_2) 1.55 (m, 1H, CH_2CH=CMe_2), 1.81 (s, 15H, C_5Me_5), 1.98 (s, 3H, $CH_2CH{=}CMe_2$), 1.99 (s, 3H, $CH_2CH{=}CMe_2$), 6.07 (t, $^3J_{HH}$ = 7.5, 1H, $CH_2CH{=}CMe_2$). ^{13}C APT NMR (100 MHz, C_6D_6): δ 10.8 (C_5Me_5), 16.4 (d, $^2J_{PC}$ = 14.2, $^1J_{WC}$ = 63.5, $CH_2CH{=}CMe_2$), 18.7 (d, $^1J_{PC}$ = 30.3, PMe_3), 18.9 ($CH_2CH{=}CMe_2$), 26.4 ($CH_2CH{=}CMe_2$), 104.9 (C_5Me_5), 122.5 ($CH_2CH{=}CMe_2$), 135.6 (d, $^3J_{PC}$ = 8.3, $CH_2CH{=}CMe_2$). ^{31}P NMR (162 MHz, C_6D_6): δ −23.9 (s, $^1J_{PW}$ = 204.1, WPMe_3). Anal. Calcd for $C_{18}H_{34}NOPW$: C, 43.65; H, 6.92; N, 2.83. Found: C, 43.54; H, 6.88; N, 2.85.

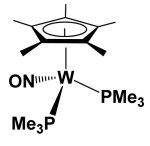

5 (15%)

Characterization data for **5** (15%): IR (cm^{-1}): 1552 (s, ν_{NO}). MS (LREI, *m/z*, probe temperature 150 °C): 501 [M^+, ^{184}W]. ^1H NMR (400 MHz, C_6D_6): δ 1.35 (d, $^2J_{PH}$ = 6.8, 18H), 1.92 (s, 15H, C_5Me_5). ^{13}C APT NMR (100 MHz, C_6D_6): δ 12.5 (C_5Me_5), 24.6 (m, PMe_3), 99.4 (C_5Me_5). ^{31}P NMR (162 MHz, C_6D_6): δ −22.2 (s, $^1J_{PW}$ = 456.8, WPMe_3).[10]

DOI: 10.1021/acs.inorgchem.5b00747
Inorg. Chem. 2015, 54, 5915−5929

Reaction of 2 with PMe_3. In a glovebox, a reaction flask was charged with **2** (0.231 g, 0.455 mmol), a magnetic stir bar, and PMe_3 (ca. 15 mL), and then the flask was sealed with a Kontes greaseless stopcock. The reaction flask was removed from the glovebox and heated in an ethylene glycol bath at 60 °C for 18 h while its contents were stirred. The flask was then allowed to cool to room temperature. Removal of excess PMe_3 in vacuo left behind a dark brown oily residue. This residue was characterized by NMR analysis and shown to contain the compounds Cp*W(NO)(H)(η^1-CH_2CH=$CHPh$)(PMe_3) (**6**), Cp*W(NO)(η^2-MeCH=CHPh)(PMe_3) (**7**), and Cp*W(NO)(PMe_3)$_2$ (**5**) in a 41:48:11 ratio. The residues were subsequently crystallized from Et_2O at ambient temperature in the glovebox to obtain reddish-orange and yellow crystals of complexes **6** and **7** that were suitable for single-crystal X-ray diffraction analyses.

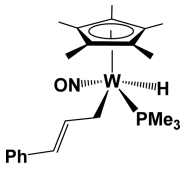

6 (41%)

Characterization data for **6** (41%): IR (cm^{-1}): 1536 (s, ν_{NO}). MS (LREI, *m/z*, probe temperature 150 °C): 543 [M^+, ^{184}W]. ^1H NMR (400 MHz, C_6D_6): δ −0.62 (dt, $^2J_{HP}$ = 80.6, $^1J_{WH}$ = 30.6, $^3J_{HH}$ = 4.3, 1H, W*H*), 1.09 (d, $^2J_{HP}$ = 8.4, 9H, WP*Me*$_3$), 1.80 (s, 15H, C_5*Me*$_5$), 1.84 (obscured, 2H, WCH_2), 6.35 (d, $^3J_{HH}$ = 15.5, 1H, PhC*H*CH), 7.01 (t, $^3J_{HH}$ = 7.4, 1H, *p*-aryl *H*), 7.13−7.27 (m, obscured, 2H, *m*-aryl *H*), 7.44 (ddd, $^3J_{HH}$ = 16.0, 9.5, 7.0, 1H, PhCHC*H*), 7.56 (d, $^3J_{HH}$ = 7.2, 2H, *o*-aryl *H*). ^{13}C APT NMR (100 MHz, C_6D_6): δ 10.5 (C_5*Me*$_5$), 17.8 (d $^1J_{CP}$ = 29.9, WP*Me*$_3$), 21.6 (d, $^2J_{CP}$ = 13.4, WCH_2), 104.7 (C_5Me$_5$), 122.2 (PhCHCH), 125.7 (*p*-aryl *C*), 125.7 (*o*-aryl *C*), 128.9 (*m*-aryl *C*), 140.4 (ipso *C*), 143.7 (d, $^3J_{CP}$ = 13.4, WCH_2CH). ^{31}P NMR (162 MHz, C_6D_6): δ −23.8 (s, $^1J_{WP}$ = 204.6, W*P*Me$_3$).

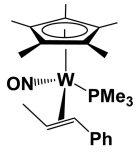

7 (48%)

Characterization data for **7** (48%): IR (cm^{-1}): 1592 (s, ν_{NO}). MS (LREI, *m/z*, probe temperature 150 °C): 543 [M^+, ^{184}W]. ^1H NMR (400 MHz, C_6D_6): δ 1.22 (d, $^3J_{PH}$ = 8.6, 9H, WP*Me*$_3$), 1.50 (d, $^4J_{PH}$ = 0.5, $^3J_{HH}$ = 6.6, 3H, PhCHCHC*H*$_3$), 1.66 (s, 15H, C_5*Me*$_5$), 2.04 (dd, $^3J_{HH}$ = 8.8, $^3J_{PH}$ = 2.4, 1H, PhC*H*), 2.48 (ddq, $^3J_{PH}$ = 11.2, $^3J_{HH}$ = 8.8, 6.6, 1H, PhCHC*H*), 6.97 (t, $^3J_{HH}$ = 7.3, 1H, *p*-aryl *H*), 7.24 (d, $^3J_{HH}$ = 7.4, 2H, *o*-aryl *H*), 7.36 (t, $^3J_{HH}$ = 7.4, 2H, *m*-aryl *H*). ^{13}C APT NMR (100 MHz, C_6D_6): δ 10.8 (C_5*Me*$_5$), 17.2 (d, $^2J_{CP}$ = 30.7, WP*Me*$_3$), 22.3 (d, $^3J_{PC}$ = 5.4, PhCHCHCH_3), 40.9 (d, $^2J_{CP}$ = 13.1, $^1J_{WC}$ = 22.8, PhC*H*CH), 50.5 (s, $^1J_{WC}$ = 35.7, PhC*H*), 104.4 (C_5Me$_5$), 123.0 (*p*-aryl *C*), 126.2 (*o*-aryl *C*), 127.7 (*m*-aryl *C*), 152.6 (ipso *C*). ^{31}P NMR (162 MHz, C_6D_6): δ −10.1 (s, $^1J_{WP}$ = 370.4, W*P*Me$_3$). Anal. Calcd for $C_{22}H_{34}NOWP$: C, 48.63; H, 6.31; N, 2.58. Found: C, 48.83; H, 6.37; N, 2.53.

Reaction of 1 with PMe_3 at 80 °C. In a glovebox, a glass bomb was charged with a sample of **1** (0.128 g, 0.305 mmol) and PMe_3 (ca. 10 mL), thereby producing a yellow solution. The bomb was sealed with a Kontes greaseless stopcock, and the stirred contents were heated at 80 °C for 18 h to obtain a dark orange mixture. The solvent was removed from the mixture in vacuo, and recrystallization of the residues from Et_2O at 20 °C afforded an orange powder (0.150 g). This powder was analyzed by ^1H and ^{31}P NMR spectroscopy and shown to contain **5** and the three isomers Cp*W(NO)(η^2-MeCH=CMe_2)(PMe_3) (**8a**) and Cp*W(NO)(η^2-CH_2=CHCHMe_2)(PMe_3) (**8b**, **8c**). Attempts to separate **5** (63%) and **8** by fractional recrystallization were unsuccessful, and the complexes decomposed during attempted column chromatographies.

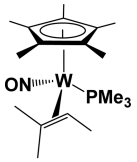

8a (17%)

Characterization data for **8a** (16.8%): MS (LREI, *m/z*, probe temperature 150 °C): 495 [M^+, ^{184}W]. ^1H NMR (400 MHz, C_6D_6): δ 1.02 (qd, $^3J_{HH}$ = 6.3, $^3J_{PH}$ = 2.5, 1H, =C*H*Me), 1.28 (d, $^2J_{PH}$ = 8.2, 9H, P*Me*$_3$), 1.37 (obscured, 3H, =C*Me*$_2$), 1.70 (s, 15H, C_5*Me*$_5$), 2.10 (d, $^3J_{HH}$ = 6.5, 3H, =CH*Me*), 2.12 (s, 3H, =C*Me*$_2$). ^{13}C APT NMR (100 MHz, C_6D_6): δ (selected signals) 11.1 (C_5*Me*$_5$), 19.2 (d, $^2J_{PC}$ = 28.0, P*Me*$_3$), 19.7 (d, $^3J_{PC}$ = 1.0, =CH*Me*), 29.9 (d, $^3J_{PC}$ = 4.6, =C*Me*$_2$), 45.8 (d, $^1J_{WC}$ = 35.8, =CHMe), 104.1 (C_5Me$_5$). ^{31}P NMR (162 MHz, C_6D_6): δ −15.2 (s, $^1J_{PW}$ = 373, W*P*Me$_3$).

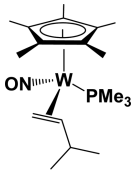

8b (11%)

Characterization data for **8b** (11.4%): ^1H NMR (400 MHz, C_6D_6): δ 0.40 (ddd, $^3J_{HH}$ = 11.3, $^3J_{PH}$ = 11.2, $^2J_{HH}$ = 4.1, 1H, =CH_2), 0.73 (dddd, $^3J_{HH}$ = 11.4, $^3J_{HH}$ = 11.3, $^3J_{PH}$ = 7.6, $^3J_{HH}$ = 1.7, 1H, =C*H*), 0.92 (d, $^3J_{HH}$ = 6.4, 3H, CHMe_2), 1.22 (d, $^2J_{PH}$ = 8.3, 9H, P*Me*$_3$), 1.47 (m, 1H, =CH_2), 1.56 (d, $^3J_{HH}$ = 6.4, 3H, CHMe_2), 1.65 (s, 15H, C_5*Me*$_5$), 2.54 (m, 1H, C*H*CMe$_2$). ^{13}C APT NMR (100 MHz, C_6D_6): δ 10.8 (C_5*Me*$_5$), 17.6 (d, $^2J_{PC}$ = 29.4, P*Me*$_3$), 18.8 (CHC*Me*$_2$), 18.9 (=CH_2), 32.1 (CHC*Me*$_2$), 32.7 (d, $^3J_{PC}$ = 4.6, *C*HCMe$_2$), 51.2 (d, $^2J_{PC}$ = 12.0, $^1J_{WC}$ = 12.0, =CH), 103.33 (C_5Me$_5$). ^{31}P NMR (162 MHz, C_6D_6): δ −13.4 (s, $^1J_{PW}$ = 372, W*P*Me$_3$).

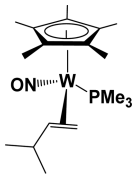

8c (9%)

Characterization data for **8c** (8.9%): ^1H NMR (400 MHz, C_6D_6): δ −0.06 (ddd, $^3J_{HH}$ = 9.4, $^3J_{PH}$ = 5.5, $^2J_{HH}$ = 4.6, 1H, =CH_2), 1.19 (d, $^2J_{PH}$ = 8.5, 9H, P*Me*$_3$), 1.28 (obscured, 1H, =C*H*), 1.30 (m, 1H, =CH_2), 1.42 (d, $^3J_{HH}$ = 6.1, 3H, CHMe_2), 1.52 (d, $^3J_{HH}$ = 5.7, 3H, CHMe_2), 1.57 (obscured, 1H, C*H*Me$_2$), 1.68 (s, 15H, C_5*Me*$_5$). ^{13}C APT NMR (100 MHz, C_6D_6): δ (selected signals) 10.9 (C_5*Me*$_5$), 16.6 (d, $^2J_{PC}$ = 31.7, P*Me*$_3$), 31.2 (d, $^2J_{PC}$ = 12.0, $^1J_{WC}$ = 17.5, =CH_2), 39.8 (*C*HCMe$_2$), 51.8 ($^1J_{WC}$ = 41.4, =CH), 103.28 (C_5Me$_5$). ^{31}P NMR (162 MHz, C_6D_6): δ −11.1 (s, $^1J_{PW}$ = 358, W*P*Me$_3$).

Reaction of 3 with PMe_3. In a glovebox, a glass bomb was charged with **3** (0.088 g, 0.22 mmol) and PMe_3 (ca. 5 mL) to produce a dark yellow mixture. The Schlenk flask was sealed with a Kontes greaseless stopcock, and its stirred contents were heated at 60 °C for 3 days, whereupon no color change occurred. The PMe_3 was then removed in vacuo, and the residue was dissolved in C_6D_6 and analyzed by ^1H and ^{31}P NMR spectroscopies to reveal the existence of four new organometallic complexes that were identified as the trapped 16e η^2-alkene complexes, Cp*W(NO)(η^2-CH_2=$CHCH_2Me$)(PMe_3) (**9a**, **9b**, **9d**) and Cp*W(NO)(η^2-MeCH=CHMe)(PMe_3) (**9c**) and complex **5** in a 41:26:25:5:3 ratio, respectively. Recrystallization of the residue by slow evaporation in the glovebox at room temperature from a 1:2 Et_2O/pentane solution afforded **9** as an orange crystalline solid (86 mg, 73% yield).

DOI: 10.1021/acs.inorgchem.5b00747
Inorg. Chem. 2015, 54, 5915−5929

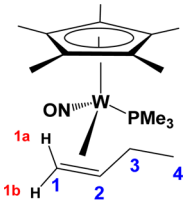

9a (41%)

Characterization data for **9a** (41%): IR (cm^{-1}): 1651 (m, υ_{NO}). MS (LREI, *m*/*z*, probe temperature 150 °C): 481 [M^+, ^{184}W], 425 [M^+ − (H_2C═CH-CH_2Me), ^{184}W]. ^1H NMR (400 MHz, C_6D_6): δ 0.35 (m, 1H, C3H_2), 0.36 (m, 1H, *H*1a), 1.23 (d, $^2J_{PH}$ = 8.0, 9H, P*Me*$_3$), 1.40 (m, 3H, C4H_3), 1.72 (s, 15H, C_5*Me*$_5$), 1.84 (m, 1H, C3H_2), 2.13 (m, 1H, C2*H*), 2.14 (m, 1H, *H*1b). ^{13}C APT NMR (100 MHz, C_6D_6): δ 11.3 (C_5*Me*$_5$), 17.7 (d, $^1J_{PC}$ = 30.3, P*Me*$_3$), 22.5 (d, $^4J_{PC}$ = 1.4, C4H_3), 27.4 (s, $^1J_{WC}$ = 37.2, C1H_2), 31.2 (d, $^3J_{PC}$ = 4.6, C3H_2), 44.6 (d, $^2J_{PC}$ = 12.0, $^1J_{WC}$ = 22.1, C2H), 103.9 (C_5Me$_5$). ^{31}P NMR (162 MHz, C_6D_6): δ −12.0 (s, $^1J_{WP}$ = 372.6, W*P*Me$_3$).

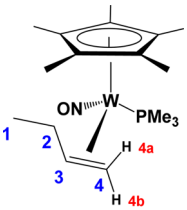

9b (27%)

Characterization data for **9b** (27%): ^1H NMR (400 MHz, C_6D_6): δ 0.09 (m, 1H, *H*4a), 1.20 (d, $^2J_{PH}$ = 8.6, 9H, P*Me*$_3$), 1.37 (m, 1H, *H*4b), 1.39 (m, 1H, C3*H*), 1.43 (m, 3H, C1H_3), 1.69 (s, 15H, C_5*Me*$_5$), 1.94 (m, 1H, C2H_2), 2.56 (m, 1H, C2H_2). ^{13}C APT NMR (100 MHz, C_6D_6): δ 10.8 (C_5*Me*$_5$), 16.8 (d, $^1J_{PC}$ = 31.7, P*Me*$_3$), 19.4 (C1H_3), 31.8 (d, $^2J_{PC}$ = 11.5, $^1J_{WC}$ = 19.3, C4H_2), 33.9 (C2H_2), 45.0 ($^1J_{WC}$ = 41.4, C3H), 103.2 (C_5Me$_5$). ^{31}P NMR (162 MHz, C_6D_6): δ −11.5 (s, $^1J_{WP}$ = 358.7, W*P*Me$_3$).

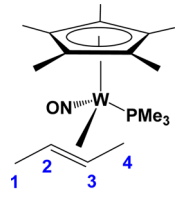

9c (26%)

Characterization data for **9c** (26%): ^1H NMR (400 MHz, C_6D_6): δ 1.07 (m, 1H, C2*H*), 1.26 (d, $^2J_{PH}$ = 8.6, 9H, P*Me*$_3$), 1.42 (m, 3H, C4H_3), 1.73 (s, 15H, C_5*Me*$_5$), 1.88 (m, 1H, C3*H*), 2.26 (d, $^3J_{HH}$ = 5.87, 3H, C1H_3). ^{13}C APT NMR (100 MHz, C_6D_6): δ 11.1 (C_5*Me*$_5$), 18.0 (d $^1J_{PC}$ = 30.3, P*Me*$_3$), 22.0 (d, $^3J_{PC}$ = 5.5, C4H_3), 25.9 (C1H_3), 41.0 (d, $^2J_{PC}$ = 12.0, $^1J_{WC}$ = 21.1, C3H), 44.0 ($^1J_{WC}$ = 38.6, C2H), 103.9 (C_5Me$_5$). ^{31}P NMR (162 MHz, C_6D_6): δ −11.4 (s, $^1J_{WP}$ = 369.9, W*P*Me$_3$).

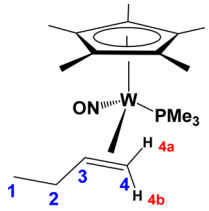

9d (5%)

Characterization data for **9d** (5%): ^1H NMR (400 MHz, C_6D_6): δ (selected signals) 0.62 (m, 1H, C3*H*), 1.25 (d, $^1J_{CH}$ = 8.6, 9H, P*Me*$_3$), 1.65 (s, 15H, C_5*Me*$_5$), 2.24 (m, 1H, H4a). ^{13}C APT NMR (100 MHz, C_6D_6): δ (selected signals) 10.4 (s, C_5*Me*$_5$), 16.1 (d, $^1J_{PC}$ = 35.9, P*Me*$_3$), 34.0 (d, $^2J_{PC}$ = 4.7, *C*4H_2), 44.9 (s, *C*3H), 103.4 (s, C_5Me$_5$).^{31}P NMR (162 MHz, C_6D_6): δ −14.8 (s, $^1J_{WP}$ = 370.6, W*P*Me$_3$).

Spectroscopic Identification of Cp*W(NO)(H)(η^1-CH_2CH═CH_2Me)(PMe_3). In a glovebox, a glass bomb was charged with **3** (0.087g, 0.21 mmol) and PMe_3 (ca. 5 mL) to obtain a dark yellow mixture. The bomb was sealed with a Kontes greaseless stopcock, and its stirred contents were heated at 60 °C for 18 h. The PMe_3 was then removed in vacuo, and the residue was dissolved in benzene-d_6 and analyzed by ^1H and ^{31}P NMR spectroscopy. The four isomers of **9**, complex **5**, and a new organometallic complex, Cp*W(NO)(H)(η^1-CH_2CH═CH_2Me)(PMe_3) (**10**), were identified in a 93:2:5 ratio, respectively.

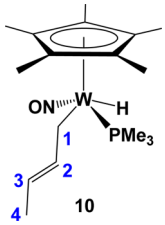

10

Characterization data for **10**: ^1H NMR (400 MHz, C_6D_6): δ −0.81 (dt, $^3J_{HH}$ = 4.7, $^2J_{PH}$ = 80.5, $^1J_{WH}$ = 30.7, 1H, W*H*), 1.09 (d, $^2J_{PH}$ = 8.5, 9H, P*Me*$_3$), 1.57 (m, 2H, C1H_2), 1.79 (s, 15H, C_5*Me*$_5$), 1.86 (m, 3H, C4H_3), 5.32 (dqt, $^4J_{HH}$ = 1.3, $^3J_{HH}$ = 15.0, 6.4, 1H, C3*H*), 6.50 (dtq, $^4J_{HH}$ = 1.4, $^3J_{HH}$ = 15.0, 7.8, 1H, C2*H*). ^{13}C APT NMR (100 MHz, C_6D_6): δ 10.8 (C_5*Me*$_5$), 18.2 (d, $^1J_{PC}$ = 29.4, P*Me*$_3$), 21.1 (d, $^2J_{PC}$ = 14.2, *C*1), 78.6 (*C*4), 104.8 (C_5Me$_5$), 116.7 9 (*C*3), 143.1 (d, $^3J_{PC}$ = 7.4, *C*2). ^{31}P NMR (162 MHz, C_6D_6): δ −24.0 (d, $^2J_{HP}$ = 85.6, $^1J_{WP}$ = 203.1, *P*Me$_3$).

X-ray Crystallography. Data collection was carried out at −173.0 ± 2 °C on a Bruker X8 APEX II diffractometer with graphite-monochromated Mo Kα radiation or at −183.0 ± 1 °C on a Bruker APEX DUO diffractometer equipped with a TRIUMPH curved-crystal monochromator using Mo−Kα radiation.

Data for **1** were collected to a maximum 2θ value of 60.34° in 0.5° oscillations. The structure was solved by direct methods[11] and expanded using Fourier techniques. All non-hydrogen atoms were refined anisotropically. Hydrogen atoms H1, H11a, H11b, and H12 were refined isotropically, and all other hydrogen atoms were included in fixed positions. The final cycle of full-matrix least-squares analysis was based on 4505 observed reflections and 186 variable parameters.

Data for **2** were collected to a maximum 2θ value of 54.964° in 0.5° oscillations. The structure was solved by direct methods[11] and expanded using Fourier techniques. The C11−C19 fragment was disordered in two orientations. All non-hydrogen atoms were refined anisotropically. Hydrogen atom H1 was refined isotropically, and all other hydrogen atoms were included in fixed positions. The final cycle of full-matrix least-squares analysis was based on 3817 observed reflections and 256 variable parameters.

Data for **3** were collected to a maximum 2θ value of 61.1° in 0.5° oscillations. The structure was solved by direct methods[11] and expanded using Fourier techniques. All non-hydrogen atoms were refined anisotropically. Hydrogen atoms H1, H12, H13, H14a, and H14b were refined isotropically, and all other hydrogen atoms were included in fixed positions. The final cycle of full-matrix least-squares analysis was based on 4354 observed reflections and 179 variable parameters.

Data for **4** were collected to a maximum 2θ value of 54.98° in 0.5° oscillations. The structure was solved by direct methods[11] and expanded using Fourier techniques. All non-hydrogen atoms were refined anisotropically. Hydrogens H1, H11A, H11B, and H12 were refined isotropically. All other hydrogen atoms were included in fixed positions. The final cycle of full-matrix least-squares analysis was based on 4619 observed reflections and 224 variable parameters.

Data for **6** were collected to a maximum 2θ value of 60.12° in 0.5° oscillations. The structure was solved by direct methods[11] and expanded using Fourier techniques. The complex crystallizes with two crystallographically independent molecules in the asymmetric unit. All non-hydrogen atoms were refined anisotropically. All hydrogen atoms

DOI: 10.1021/acs.inorgchem.5b00747
Inorg. Chem. 2015, 54, 5915−5929

were placed in calculated positions. A residual electron density peak consistent with a W−H linkage was not located; however, there was an open coordination site at both tungsten atoms consistent with the existence of a metal hydrogen linkage. The empirical formula, and any values derived from it, included this hydride, although it did not appear in the model. The final cycle of full-matrix least-squares analysis was based on 13 009 observed reflections and 484 variable parameters.

Data for **7** were collected to a maximum 2θ value of 54.964° in 0.5° oscillations. The structure was solved by direct methods[11] and expanded using Fourier techniques. All non-hydrogen atoms were refined anisotropically. Hydrogens H12 and H13 were refined isotropically, and all other hydrogen atoms were included in fixed positions. The final cycle of full-matrix least-squares analysis was based on 4939 observed reflections and 244 variable parameters.

For each structure, neutral-atom scattering factors were taken from Cromer and Waber.[12] Anomalous dispersion effects were included in F_{calc};[13] the values for $\Delta f'$ and $\Delta f''$ were those of Creagh and McAuley.[14] The values for mass attenuation coefficients were those of Creagh and Hubbell.[15] All calculations were performed using either SHELXL-97[16] via the WinGX interface[17] or XL[18] via the OLEX interface.[19] X-ray crystallographic data for all six structures are presented in Table S1 in the Supporting Information, as are full details of all crystallographic analyses.

COMPUTATIONAL METHODS

Density functional theory[20] was applied to determine the structural and energetic features of the various organometallic complexes described in this Article. All theoretical calculations were performed using Gaussian 09 (version D.01).[21] Unless specified otherwise, the 6-31+G(d) basis set[22] was used for all atoms (C, H, O, N) except W, which was treated using the Stuttgart pseudopotential and associated basis set.[23] The hybrid exchange correlation functional PBE0 was also used.[24] All structures were calculated without any geometrical constraints, and all stationary points were characterized as minima or transition states by frequency calculations. Solvent effects (specifically *n*-pentane) were included in all structure-optimization and frequency calculations using the PCM solvation model of Tomasi et al. as implemented in the Gaussian code.[25a,b] No explicit solvent modeling was required due to the extremely low coordinating properties of the hydrocarbon solvents involved in the modeled reactions. Since all tungsten complexes investigated were diamagnetic, all corresponding structures were consequently optimized in the singlet spin state. All charges were computed using an NBO partition analysis.[26]

ASSOCIATED CONTENT

Supporting Information

Table of X-ray crystallographic data for complexes **1**, **2a**/**2b**, **3**, **4**, **6**, and **7**, optimized structure and final thermochemical parameters of the various CpW(NO)(R)(η^3-allyl) complexes subjected to DFT calculations (PDF), and CIF files providing full details of the crystallographic analyses of complexes **1**, **2a**/**2b**, **3**, **4**, **6**, and **7**. The Supporting Information is available free of charge on the ACS Publications website at DOI: 10.1021/acs.inorgchem.5b00747.

AUTHOR INFORMATION

Corresponding Author

*E-mail: legzdins@chem.ubc.ca (P.L.).

Notes

The authors declare no competing financial interest.

ACKNOWLEDGMENTS

We are grateful to The Dow Chemical Company for continuing financial support of our work and to our Dow colleagues, Andy Arthur, Brian Kolthammer, Billy Bardin, and Brandon Rodriguez, for assistance and helpful discussions. We also thank Kevan Dettelbach and Tommy Tran for their contributions during the early stages of these investigations. R.A.B. acknowledges NSERC of Canada for the award to him of a PGSD postgraduate scholarship. This research has been enabled by the use of WestGrid computing resources, which are funded in part by the Canada Foundation for Innovation, Alberta Innovation, Science BC Advanced Education, and the participating research institutions. WestGrid equipment is provided by IBM, Hewlett-Packard, and SGI.

REFERENCES

(1) Baillie, R. A.; Legzdins, P. *Acc. Chem. Res.* **2014**, *47*, 330.
(2) Baillie, R. A.; Tran, T.; Lalonde, K. M.; Tsang, J. Y. K.; Thibault, M. E.; Patrick, B. O.; Legzdins, P. *Organometallics* **2012**, *31*, 1055.
(3) (a) Greenhough, T. J.; Legzdins, P.; Martin, D. T.; Trotter, J. *Inorg. Chem.* **1979**, *18*, 3268. (b) Harrison, D. P.; Nichols-Nielander, A. C.; Zottig, V. E.; Strausberg, L.; Salomon, R. J.; Trindle, C. O.; Sabat, M.; Gunnoe, T. B.; Iovan, D. A.; Myers, W. H.; Harman, W. D. *Organometallics* **2011**, *30*, 2587.
(4) Villanueva, L. A.; Ward, Y. D.; Lachicotte, R.; Liebeskind, L. S. *Organometallics* **1996**, *15*, 4190.
(5) Tsang, J. Y. K.; Buschhaus, M. S. A.; Fujita-Takayama, C.; Patrick, B. O.; Legzdins, P. *Organometallics* **2008**, *27*, 1634.
(6) Computational details: PBE0; 6-31+G(d) (C,O,N); 6-311+G(d,p) (H); SDD + Frenking *f* polarization orbitals W + pseudopotential; modelling of *n*-pentane as a solvent using PCM method; all charges computed using NBO partition scheme. See: Ehlers, A. W.; Böhme, S.; Dapprich, A.; Gobbi, A.; Höllwarth, A.; Jonas, V.; Köhler, K. F.; Stegmann, R.; Veldkamp, A.; Frenking, G. *Chem. Phys. Lett.* **1993**, *208*, 111.
(7) Armarego, W. L. F.; Chai, C. L. L. *Purification of Laboratory Chemicals*, 5th ed.; Elsevier: Amsterdam, 2003.
(8) Pamplin, C. B.; Legzdins, P. *Acc. Chem. Res.* **2003**, *36*, 223.
(9) Dryden, N. H.; Legzdins, P.; Batchelor, R. J.; Einstein, F. W. B. *Organometallics* **1991**, *10*, 2077.
(10) The existence of the complex Cp*W(NO)(PMe_3)$_2$ has been mentioned previously, but complete characterization data have not been reported; see: (a) Legzdins, P.; Martin, J. T.; Einstein, F. W. B.; Jones, R. H. *Organometallics* **1987**, *6*, 1826. (b) Lee, K.; Legzdins, P.; Pamplin, C. B.; Patrick, B. O.; Wada, K. *Organometallics* **2005**, *24*, 638.
(11) SIR-92: Altomare, A.; Cascarano, G.; Giacovazzo, C.; Guagliardi, A. *J. Appl. Crystallogr.* **1993**, *26*, 343.
(12) Cromer, D. T.; Waber, J. T. *International Tables for X-ray Crystallography*; The Kynoch Press: Birmingham, U.K., 1974; Vol. *IV*, Table 2.2 A.
(13) Ibers, J. A.; Hamilton, W. C. *Acta Crystallogr.* **1964**, *17*, 781.
(14) Creagh, D. C.; McAuley, W. J. *International Tables for X-ray Crystallography*; Kluwer Academic Publishers: Boston, 1992; Vol. *C*, Table 4.2.6.8.
(15) Creagh, D. C.; Hubbell, J. H. *International Tables for X-ray Crystallography*; Kluwer Academic Publishers: Boston, 1992; Vol. *C*, Table 4.2.4.3.
(16) SHELXL-97: Sheldrick, G. M. *Acta Crystallogr.* **2008**, *A64*, 112.
(17) WinGX − V1.70: Farrugia, L. J. *J. Appl. Crystallogr.* **1999**, *32*, 837.
(18) XL: Sheldrick, G. M. *Acta Crystallogr.* **2008**, *A64*, 112.
(19) OLEX2 − V1.2.6: Dolomanov, O. V.; Bourhis, L. J.; Gildea, R. J.; Howard, J. A. K.; Puschmann, H. *J. Appl. Crystallogr.* **2009**, *42*, 339.
(20) Parr, R. G.; Yang, W. *Density-Functional Theory of Atoms and Molecules*; Oxford University Press: Oxford, U.K., 1989.
(21) Frisch, M. J.; et al. *Gaussian 09*, Revision D.01; Gaussian, Inc.: Wallingford, CT, 2013.
(22) Krishnan, R.; Binkley, J. S.; Seeger, R.; Pople, J. A. *J. Chem. Phys.* **1980**, *72*, 650.
(23) Szentpály, L. V.; Fuentealba, P.; Preuss, H.; Stoll, H. *Chem. Phys. Lett.* **1982**, *93*, 555.
(24) Adamo, C.; Barone, V. *J. Chem. Phys.* **1999**, *110*, 6158.

DOI: 10.1021/acs.inorgchem.5b00747
Inorg. Chem. 2015, 54, 5915−5929

(25) (a) Miertuš, S.; Scrocco, E.; Tomasi, J. *Chem. Phys.* **1981**, *55*, 117. (b) Scalmani, G.; Frisch, M. J.; Mennucci, B.; Tomasi, J.; Cammi, R.; Barone, V. *J. Chem. Phys.* **2006**, *124*, 094107.
(26) Foster, J. P.; Weinhold, F. *J. Am. Chem. Soc.* **1980**, *102*, 7211.

DOI: 10.1021/acs.inorgchem.5b00747
Inorg. Chem. 2015, 54, 5915−5929